2016-05-01

Role for Reactive Oxygen Species in Methamphetamine Modulation of Dopamine Release in the Striatum

David Matthew Hedges
Brigham Young University

Role for Reactive Oxygen Species in Methamphetamine Modulation of Dopamine Release in the Striatum

David Matthew Hedges

A dissertation submitted to the faculty of
Brigham Young University
in partial fulfillment of the requirements for the degree of

Doctor of Philosophy

Richard K. Watt, Chair
Scott C. Steffensen
Dixon J. Woodbury
Joshua L. Andersen
Joshua L. Price

Department of Chemistry and Biochemistry

Brigham Young University

May 2016

ABSTRACT

Role for Reactive Oxygen Species in Methamphetamine Modulation of Dopamine Release in the Striatum

David Matthew Hedges
Department of Chemistry and Biochemistry, BYU
Doctor of Philosophy

Methamphetamine (METH) is a highly addictive substance that is highly prevalent in today's society, with over 1 in 20 adults over 26 having taken it at least once. While it is known that METH, a common psychostimulant, acts on both the mesolimbic dopamine (DA) and nigrostriatal DA systems by affecting proteins involved in DA reuptake and vesicular packaging, the specific mechanism of what is known as METH neurotoxicity remains obscure, but has been shown to involve oxidative stress. Studies have shown that reactive oxygen species act on the same proteins that METH affects. Oxidative species have also been known to catalyze the formation of melanins in dopaminergic cells. We explore this link more fully here. In an *in vitro* system, oxidative species (including Fe^{3+}, an inorganic catalyst for oxidative stress), enhance the rate of melanization of DA. Methamphetamine increased oxidative stress in an *in vivo* model. Additionally, METH enhanced phasic (stimulated) DA release and caused an electrically-independent efflux of DA. Lidocaine abolished phasic DA release, but did not affect METH-induced DA efflux, indicating action-potential dependent and independent mechanisms behind METH's effects. The sigma-1 receptor antagonist BD 1063 significantly attenuated METH's effect on DA release. Depletion of intracellular calcium (Ca^{2+}) reserves also attenuated METH-enhancement of DA release. We investigated the role of oxidative species in METH-induced DA efflux. Reduced glutathione (the substrate for glutathione peroxidase) and 4-hydroxy-TEMPOL (a superoxide dismutase mimetic) blocked METH's effect on DA release, suggesting that a reactive oxygen species (ROS), most likely superoxide, is necessary for METH-induced DA efflux. Finally, oxidative stress as well as acute METH impairs the vesicular monoamine transporter 2 (VMAT2) by S-glutathionylation modification of Cys-488, highlighting VMAT2 as a likely regulator of METH's effects on electrically independent DA release. These findings help outline a model in which METH induces DA release in the NAc through a signaling cascade involving the sigma receptor and ROS signaling molecules.

Keywords: dopamine release, methamphetamine, reactive oxygen species, neuromelanin, nucleus accumbens, voltammetry

ACKNOWLEDGEMENTS

This research has been funded by the National Institutes of Drug Abuse and Alcoholism and Alcohol Abuse. Without their support, none of our hypotheses could have amounted to anything. Additionally, BYU Graduate Studies has provided considerable support through the Graduate Studies Fellowship and the Department of Chemistry and Biochemistry has been instrumental in organizing and guaranteeing funding.

It would be inappropriate to not acknowledge the continued, behind-the-scenes support that my wife, Kaitlyn, has provided over the years. She has inspired me to try, guided me through failure, and given me the confidence to believe in success. My parents, through their expectations and confidence, have also been highly influential.

I am grateful to my committee for their suggestions and guidance. Many of them have been mentors by word, but more importantly, by example. They have taught me what it means to be a passionate research scientist, while also being a balanced individual. In particular, I am grateful to Dr. Wood, who first inspired me to seek a degree in Biochemistry and Richard Watt, who made this all possible.

I am indebted to our collaborators for their contributions. In particular, to Rick Bellinger for getting me involved with meth, Joachim Uys for his expertise in oxidative stress, and above all, to Jordan Yorgason: he wrote the software, critiqued our findings, and taught me that there is nothing like a good burger in a time of stress.

Finally, I would like to thank Scott Steffensen for his example and kindness. Without his guidance, willingness to try out bizarre ideas, and kilos of chocolate, none of this would have been possible.

TABLE OF CONTENTS

LIST OF FIGURES

LIST OF ABBREVIATIONS USED

ASC = Ascorbate

CPA = Cyclopiazonic Acid

DA = Dopamine

DAT = Dopamine Transporter

DOPAL = 3,4-dihydroxyphenylacetaldehyde

GABA = Gamma Amino Butyric Acid

GLU = Glutamate

GPx = Glutathione Peroxidase

GSH = Reduced Glutathione

METH = Methamphetamine

NAc = Nucleus Accumbens

NM = Neuromelanin

PD = Parkinson's disease

ROS = Reactive Oxygen Species

RNS = Reactive Nitrogen Species

σ1R = Sigma 1 Receptor

SNc = Substantia Nigra pars compacta

TEMPOL = 4-hydroxy-2,2,6,6-tetramethylpiperidine 1-oxyl

VMAT2 = Vesicular Monoamine Transporter 2

VTA = Ventral Tegmental Area

8-OHG = 8-Hydroxyguanosine

1 INTRODUCTION

This report is divided along two lines of investigation, with both parts looking at the effects of reactive oxygen species (ROS). The first part looks at the chemical conversion of dopamine (DA) to melanin. Neuromelanin is unique to DA neurons of the substantia nigra, and it appears to form from DA molecules in response to oxidative stress. The second part investigates the mechanism of action underlying methamphetamine (METH) enhancement of DA transmission which is thought to lead to the addictive nature of METH. Methamphetamine is known to dramatically increase ROS levels in tissue and here we show that this formation of ROS is directly related to altered DA transmission. Overall, both aspects of this study look at the effects of ROS on DA and the DA systems.

1.1 The Mesolimbic Dopamine System

The mesolimbic DA system in the mammalian brain projects from the ventral tegmental area (VTA) to structures associated with the limbic system, especially the nucleus accumbens (NAc). This system has been implicated in the rewarding effects of drugs of abuse [4-7], [8, 9]. The VTA is a relatively amorphous midbrain structure that contains at least three neuron types: primary type or dopamine (DA) neurons that project to the nucleus accumbens, secondary type or GABA neurons that may participate in local circuitry (acting to inhibit DA neurons) or project to other brain regions, and a small population of glutamatergic (GLUergic) neurons [10].

Dopaminergic neurons represent approximately 65%, GABAergic neuron about 30%, and GLUergic neurons represent about 5% of the neurons in the VTA [11, 12].

Functionally, the NAc can be divided into two structures: the core, and the shell. Current thinking is that the NAc shell is more important than the core for drug reward [13]. Rats are more likely to self-administer psychostimulant agonists into the shell than into the core [14-16]. Additionally, conditioned place preference associated with psychostimulant administration can be ameliorated by lesions in the shell, as opposed to the core [17-19]. The core appears to be more involved in conditioned responses [20-22], impulsivity [23], and responding to motivational stimuli [24-26]. Despite the functional differences, proper function of both the core and shell are necessary to mediate learning and reinforcement of Pavlovian cues [25].

Many drugs of abuse act in both the VTA and the NAc. However, most rats and mice will self-administer cocaine [27, 28], ethanol [29, 30], nicotine [31-33], cannabinoids [34], and opiates [35-38] into the VTA, suggesting that DA neurons in the VTA projecting to the shell of the NAc, and the GABA neurons that may inhibit DA neurons locally in the VTA, play an important role in mediating addiction to various drugs of abuse.

Dopamine release in target areas of the mesolimbic system has been implicated in the rewarding properties of drugs of abuse [4-7]. The emerging view is that the dysregulated homeostasis that accompanies the development of drug addiction may result from experience-dependent neuroadaptations that hijack normal synaptic transmission in the mesolimbic DA system [39-42], leading to abnormally high DA in this system [43, 44], and abnormally low DA release during periods of abstinence [45], ultimately driving drug-seeking behavior [46]. For more complete review, see Steffensen et al, 2016 [3] (**Fig. 1**).

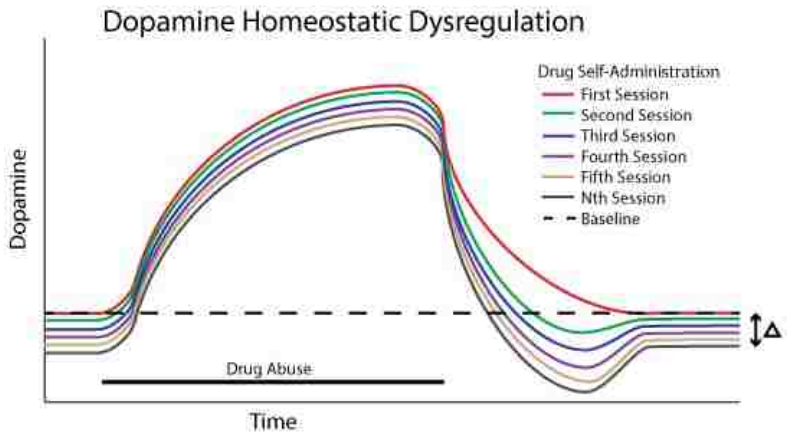

Figure 1. Model of dopamine release during and after repeated drug use.
During the first session of drug taking, DA levels in the brain are markedly increased and fall after drug binging. Dopamine levels fall after the drug session and return to pre-drug-taking levels, or baseline. The second session of drug taking is characterized by increased levels of DA, as in the first session. However, the peak increase in DA release is slightly lower, the return to baseline is slightly faster, and DA levels drop below the baseline, likely the result of homeostatic compensatory mechanisms. Dopamine levels return slowly to baseline. With each subsequent session of drug taking, the peak DA level is progressively reduced, while the kinetics of recovery are faster and the lowering below baseline is enhanced. Figure adapted from Steffensen et al, 2016 [3].

1.2 The Nigrostriatal Dopamine System

This system originates in the Substantia Nigra (in the tegmentum posterior to the VTA) and terminates in the dorsal striatum. Principally, this system is involved with initiating movement, but evidence also shows that DA release in the dorsal striatum is associated with habit formation [47]. It has been postulated that a shift from initial drug reinforcement to habit formation is demonstrated by a shift in neural circuits, possibly by a shift from NAc-related reward to dorsal striatum-mediated habit formation [48, 49].

1.3 Part 1: Dopamine Melanization

1.3.1 Melanin and Neuromelanin

Melanin is a broad term for a group of natural pigments. Melanogenesis (the formation of melanin in living tissue) results from the oxidation of amino acids or catecholamines followed by polymerization. The conversion of catecholamines to melanin is a ubiquitous process in nature. Catecholamines have been identified in 44 plant families [50, 51] and some undergo melanogenesis when the flesh of the fruit is exposed to oxygen, yielding the browning that is characteristic of rotting fruits [52]. Melanization can occur via enzymatic or catalytic reactions. In fruit, the enzymes polyphenol oxidase or catechol oxidase [53] convert catecholamines into iron-containing melanin via oxidation of catecholamines to quinones and then to melanin. There are three basic types of melanin found in humans: eumelanin, pheomelanin, and neuromelanin (NM).

The most common type of melanin, eumelanin, gives the characteristic black and brown colors of hair and skin. Melanin is a very effective absorber of ultraviolet (UV) radiation and is thought to protect skin cells (particularly their DNA) from UVB radiation damage, reducing the risk of cancer. Melanin in the skin is produced enzymatically by melanocytes converting the amino acid tyrosine to melanin via tyrosinase. However, melanocytes are also found in the eye (in both the iris pigment epithelium and in the retinal pigment epithelium), the inner ear [54, 55], and in the olfactory mucosa [56]. Disorders of melanogenesis (including albinism) result in lower levels of melanin in the skin (due to lack of functional tyrosinase), eye, ear and nose epithelium, but not in the brain. Lack of melanogenesis results in disturbances in visual, auditory and olfactory sensation and perception. In addition, albinism results in abnormal decussation of the optic nerve, nystagmus, and astigmatism [57]. Melanocytes may even play a role in some

immune responses [58]. Another melanin compound, pheomelanin, contains cysteine and is largely responsible for red and blonde hair. In the skin, melanogenesis results from exposure to UV radiation, causing the skin to visibly brown. Besides melanin's photoprotective properties, it is known to act either as a pro-oxidant or an antioxidant depending upon the degree of polymerization [59]. In the brain, melanin is found in melanocytes located in the meninges, along cerebral capillaries [60], and in the pigment epithelium in the retina.

Neuromelanin (NM) is a dark polymer pigment produced in specific populations of catecholaminergic neurons in the brain, including noradrenergic neurons in the locus coeruleus and dopaminergic (DAergic) neurons in the substantia nigra pars compacta (SNc) in the midbrain of humans and some non-human primates [61]. Parkinson's disease (PD), a relatively common neurodegenerative disease, is characterized by motor deficits such as muscle rigidity, muscle tremors, slow planned movements, and postural instability [62]. The primary cause of these motor deficits is due to the loss of DA neurons in the nigrostriatal pathway, with DA somata located in the SNc and terminals in the dorsal striatum [63]. Since it has been observed that DA neurons containing less NM are more likely to die in models of PD [64, 65] and that NM can bind to and render iron ions redox inactive [66], it has been proposed that NM has a neuroprotective role [67], possibly acting as an antioxidant.

1.3.2 Dopamine and Oxidative Stress

Based on the susceptibility of DA neurons to oxidative stress, possessing an extra mechanism for dealing with ROS would be particularly important for DA neurons. First, DA metabolism adds to generalized oxidative stress, as it generates hydroxyl radicals and 3,4-dihydroxyphenylacetaldehyde (DOPAL) when degraded by monoamine oxidase A [68, 69]. Additionally, the SNc contains higher levels of iron as compared to other brain areas [70],

around 300 μg/g [71]. These iron deposits are found in in the midbrain as well as in DA cell culture [72], indicating that iron is localized in DA somata and not just in neuroglia. Iron is a significant source of oxidative stress, particularly when combined with H_2O_2 produced from DA metabolism, creating hydroxyl radicals via the Fenton reaction [73]. Therefore, the neuroprotective effect of NM is likely due to an antioxidant feature of NM that is able to bind and inactivate redox-active iron ions [66], preventing hydroxyl radical production [74]. Neuromelanin has been shown to be a powerful chelator of neurotoxic metals and has two distinct chelation sites for Fe^{3+}, a high affinity and low affinity site [75]. In fact, NM appears to contain the largest reservoir of iron in catecholaminergic cells [76, 77].

1.4 Part 2: Methamphetamine Enhancement of Dopamine Transmission

1.4.1 The Cycle of Addiction and Treatment Strategies

A major goal of research on addiction is to characterize the critical neural substrates that are most sensitive to drugs of abuse, adapt in association with chronic consumption, and drive subsequent drug-seeking behavior. A significant need exists for understanding how drugs of abuse affect DA transmission in the mesolimbic system. The rationale for the second part of this study was predicated on the belief that advancement in the understanding of the brain mechanisms underlying the recreational use and abuse potential of methamphetamine will pave the way for more effective treatment strategies that could reverse drug dependency and save lives and resources throughout the world.

Addicts continue their cycle of abuse as a result of low dopamine (DA) levels in pleasure areas of the brain. These low levels of DA result in feelings of anxiety and dysphoria, impelling subsequent drug seeking and taking [46]. Systemic administration of psychostimulants

temporarily enhances DA levels. Current dogma states that the short-lived enhancement of DA release in the NAc and other pleasure system structures is what underlies the euphoric aspect of psychoactive drugs and natural rewarding behaviors (e.g., eating, drinking, and sex). However, drugs of abuse easily overwhelm this system and tolerance/dependence result in subsequent drug taking, ultimately causing persistent dysfunctional DA homeostasis.

Conventional therapies for addiction include self-help groups, drug therapy, and substitution therapy. The search for effective medications for substance abuse and addiction has been difficult as contemporary medications produce akinesia, deficits in cognitive performance, and disrupt natural pleasure sensation [46]. These side-effects result in an understandable lack of patient compliance and poor prognoses.

1.4.2 The Economic and Societal Costs of Methamphetamine Abuse

Widespread drug abuse, both illicit and licit, takes an enormous toll on society as well as on individual human suffering. In 2005, it was reported that METH costs the nation about $23.4 billion [78]. The consequences of drug abuse include: lost job productivity, squandered earnings, rising healthcare costs, incarcerations, investigations, vehicular accidents, domestic and non-domestic violence, premature death, and the breakdown of the family unit ("National Survey on Drug Use and Health"). The economic and societal implications arising as direct or indirect result of drug abuse consumption are staggering. In 2012, the National Survey on Drug Use and Health reported that over 12 million people have tried methamphetamine at least once, with 1.2 million users in the year preceding the survey [78]. Long-term problems of METH abuse include anxiety, confusion, insomnia, inexplicable violent behavior, mood disorders, paranoia, hallucinations, delusions, and decreased motor skills [79]. All of these side effects can negatively impact an individual's ability to maintain relationships and manage productive employment.

1.4.3 Effects of Methamphetamine on VMAT2, DAT, and the Sigma Receptor

While the physiologic effects of amphetamines have been experimented with for millennia, the specific mechanism of action is only just being understood. All accounts agree that amphetamines (including methamphetamine and MDMA) act directly on the dopamine terminals. Amphetamine has a myriad of effects that may influence DA release. As a substrate for the DA transporter (DAT) [80, 81] and vesicular monoamine transporter 2 (VMAT2) [80, 82, 83], amphetamines, including METH, disrupt neurotransmitter reuptake and repackaging, resulting in increases in evoked DA at low concentrations. Through its interactions with VMAT and vesicles, METH is thought to increase cytoplasmic levels of DA, overwhelming the DAT, and causing reverse transport of DA outside of the cell, and eventual depletion of DA stores [84-89].

A pre-dose of reserpine (an irreversible antagonist of VMAT, which packages monoamine neurotransmitters into vesicles), has been shown to decrease amphetamine-mediated release of DA by 75% [90]. In fact, later evidence suggested competition between reserpine and methamphetamine in binding to VMAT [91]. A single dose of methamphetamine has been shown to lower the rate of vesicular packaging of DA [92], further implicating VMAT as a target of methamphetamine.

However, it has also been shown that amphetamine (similar to cocaine) is able to bind to dopamine active transporter (DAT) [93]. Strangely, they found that self-administration was more effective with amphetamine than would be expected when comparing its binding affinity to DAT to that of cocaine [93].

One promising protein target for METH's effects on ROS formation is the sigma-1 receptor (σ1R). The σ1R is a ligand-gated chaperone protein which, upon activation, translocates

to various cellular compartments of the endoplasmic reticulum (ER) where it is thought to affect protein folding, function of ion-channels and G-protein coupled receptors (GPCRs), and the formation of mitochondrial sourced ROS [94-97]. Interestingly, antagonizing the σ1R prevents METH-induced ROS generation and DA release [98], suggesting that METH's actions on the σ1R may be a possible underlying mechanism behind the formation of METH-generated ROS, and subsequent DA release *in vivo*. Moreover, while selective σ1R agonists are not sufficient for driving positive reinforcement, many σ1R agonists substitute for both METH and cocaine in self-administration paradigms [94, 99], further implicating this receptor in the reinforcing effects of METH.

1.4.4 Methamphetamine Modulation of Dopamine Release: Microdialysis versus Voltammetry

Classically, measuring DA in tissue has been dominated by a technique called microdialysis, which effectively removes and replaces small volumes of cerebral spinal fluid (which contains both DA and DA metabolites) and separates particles using HPLC combined with electrochemical detection. Recently, researchers are turning to voltammetry to measure in-tissue DA (for a full description of voltammetry procedures, see Methods section). Microdialysis and voltammetry are valuable, complementary tools for measuring DA release, but they both have their inherent advantages and disadvantages. Microdialysis is able to measure extracellular DA levels with specificity, accuracy, and precision. Dopamine concentrations in the NAc fluctuate on phasic (subsecond) and tonic (minutes) timescales [100]. However, microdialysis's temporal resolution is on the order of 5-20 minutes and can be affected by changes in DA uptake [101], and its spatial resolution is limited to the size of relatively large probes. Voltammetry lacks the specificity of microdialysis, but is able to measure DA release with more precise spatial

resolution and at sub-second time resolution, and allows the added assessment of uptake kinetics. It also allows a complete analysis of phasic vs tonic release of DA, as it is possible to change the electrical evoked stimulus to different pulse trains, simulating phasic vs tonic release [102]. One clear advantage of voltammetry is the ability to study DA transients, which emulates microdialysis in some respects, as DA release is spontaneous and not evoked. Recent evidence suggests that methamphetamine alters both DA transients [103] and standard phasic DA firing and release [104]. In fact, it has been shown that methamphetamine slows phasic DA release, without affecting tonic release [105]. Taken together, these results provide compelling evidence for the need to use voltammetry to better understand the concrete pathways for methamphetamine neurotoxicity.

1.4.5 Methamphetamine and Reactive Oxygen Species

Reactive Oxygen Species (ROS) are implicated in many cellular processes. Of particular relevance are the effects of ROS on DA systems. First, decreased levels of ascorbate in the striatum are associated with Huntington's disease [106], a disorder characterized by an overabundance of DA release. Cocaine has been shown to induce the generation of free radicals in DA neurons [107], possibly by inhibiting catalase [108]. Treating rats with an antioxidant was shown to decrease cocaine-induced motion sensitization, suggesting that oxidative stress is at least partially responsible for certain behavioral changes in cocaine-treated animals [109]. Furthermore, Parkinson's disease (caused by a terminal degeneration of DA neurons in the substantia nigra) is associated with increases in iron homeostasis and the ensuing increase in oxidative stress [110].

Methamphetamine is known to drive production of ROS [111-113]. Additionally, ROS have also been shown to decrease DAT function in the striatum [114]. Taken together, these

results suggest that it is possible that the neurotoxic effects of methamphetamine on the DA systems may occur indirectly, through ROS intermediates.

Methamphetamine is known to increase metabolic function in DA neurons [115, 116], consequently raising brain temperature [116-118]. Cellular metabolism is a tightly controlled mechanism. When it becomes imbalanced (due to drug interactions or chronic health problems, etc.), the electron transport chain can start to produce ROS (free radicals and peroxides) [116]. Since mitochondria are densely concentrated near synapses [119, 120], alterations in metabolism that could spill oxidative stress into axon terminals could be particularly devastating, especially to DA neurons, which appear to be specifically targeted by methamphetamine, in that following chronic or high-dose methamphetamine exposure, damage to DA axons has been observed [121-123]. It is possible that this selective targeting of DA axon terminals may be related to methamphetamine's action on mitochondria and the ensuing increase in local oxidative stress.

All things considered, significant evidence exists supporting the role for ROS in methamphetamine neurotoxicity. Oxidative stress is known to affect one of the two principle targets of methamphetamine and methamphetamine is able to induce ROS formation. Since studies have shown that blocking ROS can ameliorate the transient DA spikes following psychostimulant exposure, it is possible that initial exposure to ROS can actually increase DA release in terminal areas. Additionally, these findings indicate an interesting possibility for treatment of chronic psychostimulant users – a therapy focused on regulating oxidative stress in DA neural pathways.

Overall, this study is divided into two main parts. The first deals with the chemical effects of oxidative stress (especially resulting from iron) on the DA molecule. Oxidative stress increases the rate of melanization of DA, and it appears that the presence of melanin in DA cells

indicates past oxidative stress. The second part of this study focused on the effects of oxidative stress (especially as induced by METH) on DA transmission in the striatum. Experiments involving quantification of DA release utilized fast-scan cyclic voltammetry, measuring DA in the striatum of C57Bl/6j mice. For greater detail, see the Methods section.

2 METHODS

2.1 Experimental Animals and Animal Care

Animals for experimentation were obtained through Dr. Steffensen's established rodent colonies. The utilization of mice for methamphetamine studies was to better approximate the therapeutic model on humans.

C57BL6 mice (Steffensen Laboratory, Provo, UT) weighing 25-40 grams were housed 4-5 to a cage with *ad libitum* access to food and water. The room was temperature controlled (22-25 ^{o}C) and maintained on a reverse 12 hr light/dark cycle (off 08:00 hrs, on 20:00 hrs). All care and procedures are in accordance with the National Institutes of Health *Guide for the Care and Use of Laboratory Animals* and approved by the BYU Institutional Animal Care and Use Committee.

2.2 Reagents and General Procedures

3-Hydroxytyramine (dopamine; DA) was purchased from Sigma Aldrich. Due to its reactive nature, DA solutions were prepared immediately before each experiment. The solutions that reactions were run in were: transferrin-treated double distilled H_2O (which was subsequently filtered to remove the transferrin, an iron binding protein, and any residual iron contamination – see below), intracellular fluid (ICF; consisting of: 125.0 mM KCl, 10.0 mM Hepes, 2.0 mM $MgCl_2$, and 0.5 mM $CaCl_2$), and extracellular fluid (ECF;

consisting of: 124.0 mM NaCl, 2.0 mM KCl, 1.25 mM NaH_2PO_4, 24.0 mM $NaHCO_3$, 12.0 mM Glucose, 1.2 mM $MgSO_4$, and 2.0 mM $CaCl_2$). Both ICF and ECF were bubbled with 95% O_2 / 5% CO_2 to help maintain pH 7.3. In some experiments, Mg^{2+} and Ca^{2+} were either not added or added at different concentrations, as discussed in the Results section. The concentration of DA was 30 μM in our experiments, except in specific experiments involving DA concentration-response studies. Although ECF and ICF were used as buffers to mirror both extracellular and intracellular conditions, the focus of this paper is on monitoring the chemical reaction of DA being converted to melanin within physiologic parameters, thus the role of metal ions in DA melanization was evaluated at concentrations spanning their known cellular ranges.

All other reagents were purchased from the suppliers shown in parentheses and were used at the concentrations indicated in the Results section: Sodium ascorbate (Spectrum Chemicals & Laboratory Products); Glutathione (Sigma- Aldrich); Hydrogen peroxide (Fisher Scientific); Desferrioxamine (Sigma-Aldrich); Transferrin (Lee Biosolutions).

2.3 Transferrin Treatment

To ensure that there was no iron contamination in our analysis of Ca^{2+} and Fe^{3+}, we treated molecular biology grade water (with 10 μM CO_3^{2-}, to facilitate iron loading onto transferrin) with 10 μM transferrin (transferrin binds Fe^{3+} at 10^{23} M^{-1} and has a molecular weight of 80 kDa). After incubating for 15 minutes, the solutions were loaded into Amicon Ultra-4 Centrifugal Filter Units with Ultracel-10 membrane, with a molecular cut-off at 10 kDa (EMD Millipore) and spun in a centrifuge at 4000 rpm for 15 minutes. The transferrin was retained in the upper chamber of the filter and the filtrate (purified water) was recovered from the flow-through of the filter and used for experiments.

2.4 UV-Vis Spectrophotometry (the 480 nm Assay)

Samples were placed into standard 10 mm light path quartz cuvettes (US Solid, Oakland, CA) and the full spectrum was scanned (200 nm – 900 nm) in a Thermo Scientific Biomate 3S UV-Visible Spectrophotometer (Waltham, MA). For experiments that needed to be guaranteed iron-free, two-sided plastic disposable cuvettes (VWR) were used in place of quartz. An initial scan of the sample was taken immediately after sample preparation and collections continued every 10 minutes for two hours (13 collections total). Our experiments, and those of others [1, 2], have demonstrated that the process of melanization of catecholamines can be closely monitored in its early stages by the formation of an absorbance peak at 480 nm. Over time, (and as melanin becomes less soluble), this peak becomes obscured as the spectrum approaches that of mature melanin. We have, therefore, developed a spectrophotometric assay that measures the early formation of melanin by quantifying the rate of polymerization based on the absorbance over time at 480 nm.

2.5 Slice Preparation

Experimental protocols were approved by the Institutional Animal Care and Use Committee (IACUC) of Brigham Young University which met or exceeded NIH guidelines. Adult male C57BL6 mice (post-natal day 30-120) from our own breeding colony were used in this study. Once weaned at PND 21, all mice were housed in groups of four/cage and placed on a reverse light/dark cycle with lights ON from 8 PM to 8 AM. Horizontal brain slices were obtained as previously described (31). Mice were anesthetized with ketamine (60 mg/kg, IP), decapitated, and the brains were quickly extracted and sectioned into 0.4 or 1 mm thick coronal slices in ice-cold cutting solution, bubbled with 95% O_2 / 5% CO_2. The cutting

solution consisted of 220.0 mM Sucrose, 3.0 mM KCl, 1.25 mM NaH_2CO_3, 12.0 mM $MgSO_4$, 10.0 mM Glucose, and 0.2 mM $CaCl_2$. Slices containing the striatum were immediately placed into an incubation chamber containing normal ECF bubbled with 95% O_2 / 5% CO_2. Slices were incubated for at least 30 minutes at 36°C and then transferred to a recording chamber with continuous normal ECF flow (2.0 ml/min), and the temperature was maintained at 36°C throughout the experiment via a Warner Instruments TC-344B Dual Automatic Temperature Controller (Hamden, CT).

2.6 Voltammetry

For fast scan cyclic voltammetry (FSCV) recordings, a 7.0 μm diameter carbon fiber was inserted into borosilicate glass capillary tubing (1.2 mm outer diameter; A-M Systems, Sequim, WA) under negative pressure and subsequently pulled on a vertical pipette puller (Narishige, East Meadow, NY). The carbon fiber electrode (CFE) was then cut under microscopic control with 150 μm of bare fiber protruding from the end of the glass micropipette. The CFE was back-filled with 3 M KCl. The CFE's were regularly calibrated with a known concentration of DA. With the CFE positioned in the solution of ECF, we superfused a known concentration of DA at a high flow rate (5 mL/min) past the electrode and observed the maximum nA signal produced by DA. These DA calibrations were averaged to convert a nA signal of DA oxidation to μM concentration of DA.

To observe melanization utilizing FSCV, 3.0 mL of ECF was placed in a large flow cell bath chamber (Warner Instruments, Hamden, CT) that was modified to prevent leakage (i.e., static flow system). Both a reference electrode and the CFE were positioned well below the surface of the fluid, but off the bottom of the chamber. The electrode potential was linearly

scanned as a triangular waveform from -0.4 to 1.2 V vs Ag/AgCl using a scan rate of 400 V/s. Cyclic voltammograms were recorded at the CFE every 2 seconds (i.e. 0.5 Hz) by means of a ChemClamp voltage clamp amplifier (Dagan Corporation, Minneapolis, MN). Voltammetric recordings were performed and analyzed using LabVIEW (National Instruments, Austin, TX)-based customized software (Demon Voltammetry [124]). The two-hour (or three-hour) recording was initiated without DA being present in solution (to allow for an appropriate baseline recording). Dopamine was added to the bath chamber from a stock solution (10 mM) after five minutes of baseline recording at a volume to produce 30 µM in 3.0 mL of ECF.

2.7 Stimulation and Recording

For *ex vivo* voltammetry recordings, electrodes were positioned ~75 µm below the surface of the slice in the NAc core. Dopamine release was evoked every 2 min by a 1 msec, one to ten-pulse stimulation (biphasic, 350 µA) from a micropipette tip broken to 5-10 µm, filled with ACSF and oriented 100-200 µm from the CFE. The CFE potential was linearly scanned as a triangular waveform from -0.4 to 1.2 V and back to -0.4 V vs Ag/AgCl using a scan rate of 400 V/s. Cyclic voltammograms were recorded at the CFE every 100 msec (i.e., 10 Hz) by means of a ChemClamp voltage clamp amplifier (Dagan Corporation, Minneapolis, MN). Voltammetric recordings were performed and analyzed using LabVIEW (National Instruments, Austin, TX)-based customized software (Demon Voltammetry, [124]). For calibrations, at end of experiments, CFEs were placed in bath flow with no tissue sample present. 3 µM DA was perfused in the bath solution and the resulting max current from the CFE was recorded. Dopamine currents were converted to concentration based on the average calibration ratios.

Stimulations were performed periodically every 2 min. For recording the DA efflux (action potential independent release), once the stimulated DA response was stable for five

successive collections, and did not vary by more than 5%, the electrical stimulation was turned off. Without moving the electrodes, cyclic voltammograms were recorded at 0.5 Hz for 3 hrs. For TEMPOL and GSH experiments, the antioxidants were added 30 min prior to METH application. Unless otherwise specified, all other recordings were performed with the pharmacological agent at 30 min and METH at 60 min. Since voltammetry is a background subtracted technique, all data reflect changes in DA release, and not absolute extracellular DA concentrations.

2.8 Mass Spectrometry

S-glutathionylation of purified human VMAT2 (Origene, Rockville, MD) was induced by incubation with 10 μM tetraethylthiuram disulfide (disulfiram, Sigma) in the presence of reduced L-glutathione (Sigma Aldrich) for 30 min at 37°C. The sample was loaded onto 4-12% Bis-Tris precast gels and separated by Western Blot electrophoresis using MOPS buffer (Bio-rad, Hercules, CA) and a CriterionTM Cell system (CriterionTM, Bio-rad, Hercules, CA). Following overnight staining with Proto Blue Safe (National Diagnostics), the protein band was destained, and digested for 3 hrs with Lys-C (Wako, Richmond, VA) and overnight with trypsin (Sigma Aldrich) in the presence of 1% Rapigest. The peptides were extracted and acidified to cleave the Rapigest detergent. Peptides were loaded on a trap column, eluted, and separated on a 75 μm x 15 cm fused-silica column packed in house with C18 reversed-phase resin (YMC-ODS-AQ; 5-μm particles; 120-Å pore from Waters, Milford, MA) using an acetonitrile gradient of 5-50% in 120 min containing 0.2% formic acid on a LC Packings U3000 nano LC system at flow rate of 200 nL/min. Peptides were mass analyzed by a Thermo Orbitrap Elite with collision induced dissociation (CID), higher energy collisional dissociation (HCD), and electron transfer dissociation (ETD) fragmentation capabilities. Mass spectra were acquired in data dependent

mode using an alternating CID/ETD top 10 method. One FTMS survey MS scan in the mass range of m/z 400-1700 was followed by tandem mass spectra (MS/MS) of the ten most intense precursors fragmented by both CID and ETD. All MS/MS fragments were detected in the ion trap. The automatic gain control target value in the Orbitrap was 106 for the survey MS scan at a resolution of 60,000 at m/z 400. Fragmentation in the LTQ was performed by collision induced dissociation with a target value of 10000 ions followed by ETD with no additional supplemental activation. The threshold count was 500 for both CID and ETD. Dynamic exclusion was enabled with a repeat count of 2, repeat duration of 30 sec, exclusion list of 50, and exclusion duration of 120 sec. The predominant neutral loss of γ glutamic acid (-129 Da) by CID or HCD was used to trigger the acquisition of an ETD tandem mass spectrum. With CID, disulfide bonds remain intact and fragmentation on either side of the disulfide bond results in the conversion of the disulfide linked cysteine to dehydroalanine (-33.99 Da) or persulfide (+31.97 Da). Glutathione, which increases the mass of cysteine by 305.07 Da, also undergoes fragmentation resulting in the neutral loss of γ glutamic acid (-129 Da)[2]. By electron transfer dissociation, the disulfide bond is preferentially fragmented resulting in the loss of glutathione (305) from the precursor and fragment ions and the generation of the glutathione oxonium ion at m/z 308 [125]. The automatic gain control target value in the Orbitrap was 106 for the survey MS scan at a resolution of 60,000 at m/z 400. Fragmentation in the LTQ was performed by collision induced dissociation with a target value of 10000 ions. Charge state enabled ETD reaction time was utilized and supplemental activation was turned off. An additional analysis was performed with alternating CID and ETD with supplemental activation energy enabled. The threshold count was 500 for both CID and ETD. Dynamic exclusion was enabled with a repeat count of 3, repeat duration of 30 sec, and exclusion duration of 100 sec. The CID, HCD, and ETD MS/MS spectra

were searched using MASCOT (Version 2.4.01) and SEQUEST HT search algorithms utilizing Proteome Discoverer 1.4 (Thermo Scientific, Waltham, MA). For both algorithms, the search parameters allowed for 2 missed cleavages, precursor mass tolerances of ± 10 ppm, fragment mass tolerances ± 0.8 Da, dynamic modifications on cysteines included S-glutathionylation (305 Da).

2.9 Nuclear Magnetic Resonance Studies

For NMR experiments, 30 μM DA was pipetted into standard Norrell NMR tubes (Landisville, NJ). The samples were analyzed using a Varian NMR-System 500 MHz (Agilent Technologies, Santa Clara, CA). Solutions were prepared in D_2O (Cambridge Isotope Laboratories, Andover, MA) to minimize solvent noise.

2.10 VMAT2 Activity Assay

Fresh accumbens tissue was homogenized in a sucrose Hepes buffer (320 mM sucrose, 10 mM Hepes, pH 7.4 with protease and phosphatase inhibitors) and centrifuged. The supernatant was treated with disulfiram (10 μM) and GSH (10 mM) and incubated at 37°C for 30 minutes. Samples were run through bio-spin size exclusion columns (BioRad, Hercules, CA) and 1 mM fluorescent probe was added in the dark (FFN 206, Abcam, Cambridge, MA). Fluorescence counts were determined using a plate reader (λ_{ex} = 350 nm, λ_{em} = 460nm).

2.11 VMAT2 co-Immunoprecipitation Assay and Immunoblot

Animals were divided randomly into three groups that were then double-injected with saline/saline, saline/METH (10 g/kg), and BD 1063 (30 g/kg) / METH (10 g/kg), respectively. The injections were approximately 10 minutes apart. 30 minutes after the second injection, NAc tissue

was immediately harvested and chilled. The tissue samples were lysed in ice-cold TNTE buffer (containing the following in mM: 50 Tris pH 7.4, 150 NaCl, and 1 EDTA in addition to 0.5% Triton X-100) for 10 min with a rotation at 4°C. Tissue lysates were triterated 10 times using a 23 gauge needle and cleared by centrifugation at 14800 G for 10 min. Anti-VMAT2 antibody (EMD Millipore, Billerica, MA) was coupled to magnetic dynabeads (ThermoFisher, Waltham, MA) and immunoprecipitated VMAT2 from tissue lysates according to the manufacturer's instructions. Immunoprecipitated VMAT2 was run on a 10% SDS-PAGE and immunoblotted for anti-GSH (Virogen, Watertown, MA) and anti-VMAT2 antibodies.

2.12 Drug Administration in Slice Preparation

All drugs were bath applied. Proper delivery was achieved by moving the peristaltic pump intake tube from the container containing the control solution to a container containing a predetermined concentration of the appropriate drug in control solution. Drug-free washout ACSF was administered by moving the peristaltic pump intake tube back to the container containing control ACSF.

2.13 Statistical Analyses

The results were compiled from spectrophotometers and the rate of melanization was calculated from the slope of the absorbance versus time. For FCSV experiments, peak DA oxidation currents measured via FSCV were isolated and compiled. The means were then grand-averaged across trials. Values were expressed as means±SEM for cumulated data. Between-subject group comparisons were analyzed via one-way ANOVAs. The criterion of significance was set at $p < 0.05$ (*), $p < 0.01$ (**), $p < 0.001$ (***), and $p < 0.0001$ (#). All statistics were calculated with IBM SPSS Statistics 23 (Armonk, New York).

3 RESULTS

3.1 Metal Chelation by the Dopamine Catechol can enhance the rate of Dopamine Melanization

3.1.1 Role of Initial Substrate in Rate of Melanin Formation

Dopamine in solution melanizes over time and can be tracked by measuring the change in absorbance at 480 nm (**Fig. 2A, B**). To determine if the formation of melanin was dependent on the initial concentration of DA, we examined the rate of melanization at 0.3, 3.0, and 30 μM DA (**Fig. 3 A**). These concentrations are significantly lower than vesicle concentrations [126], but are comparable to intracellular and synaptic concentrations. The rate of melanin formation was directly proportional to the initial concentration of DA in solution, with higher concentrations of DA resulting in faster rates of melanin formation (**Fig. 3A**). This relationship was linear (R^2= 0.987). Because of this linear relationship, we decided to use the 30 μM concentration as our control standard.

We then compared the rate of melanization produced by DA to that of tyrosine, L-DOPA, epinephrine, and norepinephrine at equimolar concentrations (30 μM). Dopamine showed the fastest rate of melanization when compared with the related compounds (**Fig. 3B**). Comparing all five groups via one-way ANOVA demonstrated significance between DA vs all

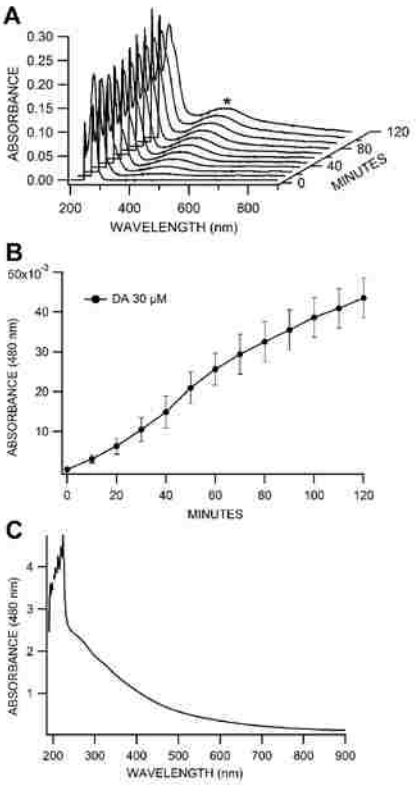

Figure 2. Spectrophotometric characterization of melanin.
(A) Waterfall plot of full spectrum (190 –900 nm) demonstrating the progressive melanization of DA in ECF. As shown by Graham, 1978 and Mosca et al, 1998, this 480 nm peak represents DA melanization [1, 2]. **(B)** This graph summarizes the kinetics of the 480 nm peak (n=8). **(C)** Characteristic spectrum of mature melanin.

four other conditions ($F(4,19)=30.734$, $p<0.0001$). Tukey post-hoc analysis did not demonstrate any significance between any groups outside of DA ($p<0.05$).

In order to verify that the 480 nm peak we were measuring with spectrophotometry was melanin or a melanin precursor (rather than some form of oxidized DA or dopaminochrome), we performed proton nuclear magnetic resonance (H-NMR) experiments of the DA solution in ECF buffer. We ran a kinetics study using H-NMR with Fe^{3+} (10 µM) present to maximize melanization. A comparison of the NMR peaks showed that the predominant species in solution at both time zero (**Fig. 4A**) and 2 hours (**Fig. 4B**) was DA (melanin is inherently insoluble and ultimately precipitates). This indicated that the colorimetric

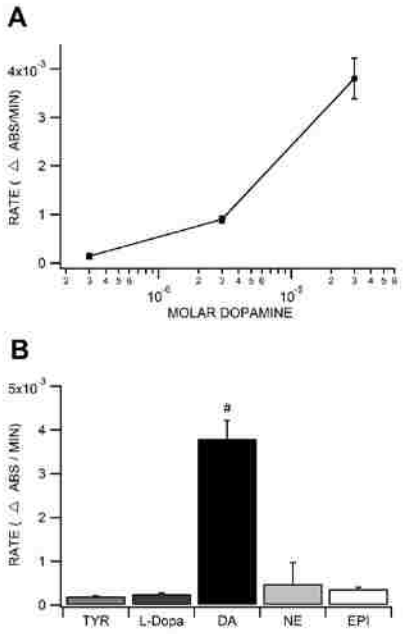

Figure 3. Chemical characterization of dopamine melanization.
(A) The rate of growth (Δ Abs/min.) of DA melanization (as given by the growth of an absorbance peak at 480 nm) is dependent on initial DA concentration. The representative rates are calculated from a two-hour collection interval. 3.0 μM DA is approximately the concentration of DA release in the striatum. 0.3 μM DA approximates intracellular (extravesicular) concentrations and 30 μM is smaller than the concentration of DA in vesicles. There is a linear relationship between the concentration and rate. **(B)** This graph demonstrates the rate of growth (Δ Abs/min.) of DA melanization to that produced by its amino acid precursors and metabolic derivatives (all at 30 μM concentration). While all species tested show a certain amount of melanization, the unique chemistry of DA allows it to polymerize at a significantly faster rate. The n values for each experiment are n=4 (tyrosine), n=4 (L-Dopa), n=8 (dopamine), n=4 (norepinephrine), and n=4 (epinephrine).

change we were tracking with the 480 nm assay was either melanin or an immediate precursor to melanin.

3.1.2 An Analysis of Physiologically Relevant Concentrations of Metals Linked with Oxidative Stress and their Effects on Melanin Synthesis

As NM has been shown to have at least two iron chelation sites and it has been proposed previously that NM may act as an iron chelation agent in DAergic neurons [76, 77], we tested iron (III) chloride at five concentrations (1.0, 10.0 nM and 0.1, 1.0, 10.0 μM) mixed with the

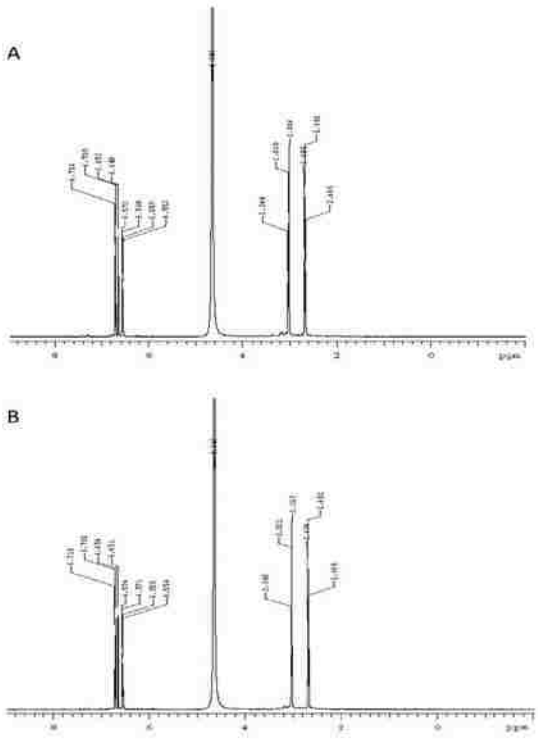

Figure 4. H-NMR analysis of dopamine pre and post melanization.
NMR traces of the beginning and end of a 2 hour experiment in which 10 µM iron was added to 30 µM DA (to catalyze melanization). **(A)** The initial H-NMR trace showing the distinctive peaks for DA. **(B)** The same sample as in A, but two hours later when the solution began to visibly darken and precipitate with the presence of melanin. The peaks are nearly identical in both collections, indicating that the major species in solution in both samples is DA.

reaction mixture (transferrin-treated ddH_2O + 30 µM DA) (**Fig. 5**). Iron significantly induced DA melanization in a concentration-dependent manner ($F_{(5,20)}$=90.812, p<0.0001).

Calcium is known to coordinate to the hydroxyl groups of catechols, like Fe^{3+}. Thus, we tested six concentrations of Ca^{2+} (0.1, 1.0, 10.0, 100 µM and 1.0, 10.0 mM Ca^{2+} in the reaction mixture – transferrin treated ddH_2O + 30 µM DA) to determine if Ca^{2+} can drive melanization. Our result show that Ca^{2+} did not significantly induce melanization ($F_{(6,20)}$= 1.201, p= 0.346).

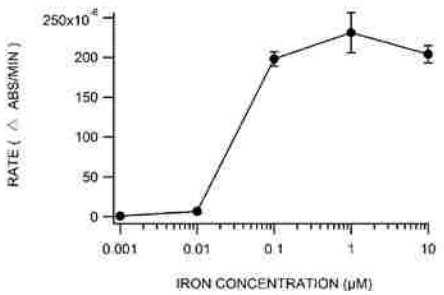

Figure 5. The effect of iron on melanin formation.
Iron increased the rate of melanization in a concentration-dependent manner in iron-free water. The curve is roughly sigmoidal. The n values for each run are n=4 (1.0 nM), n=4 (10.0 nM), n=4 (100.0 μM), n=4 (1.0 μM), and n=6 (10.0 μM).

3.2 Reactive Oxygen Species Enhance the Rate of Dopamine Melanization and Antioxidant Species can Decrease this Rate

3.2.1 An Analysis of the Effects of Radical Initiators and Quenchers on the Rate of Melanin Formation

To confirm that oxidative agents can drive the conversion of DA to melanin, we added H_2O_2 (500 μM) into the reaction mixture. This concentration of H_2O_2 increased the rate of melanization by 54.6% (**Fig. 6A**). We used an ECF buffer for this experiment as well as in the following analysis of pro- and antioxidants because preliminary studies have shown that it is a reliable buffer system to use for baseline growth and also provides a better control for our final study with KCl-evoked DA release. A one- way ANOVA showed that this increase in rate due to H_2O_2 is significant ($F(1,10)=27.422$, $p=0.0004$).

To provide a correlate for the experiment with H_2O_2, we also tested the effects of the antioxidants ascorbate (ASC) and glutathione (GSH) on DA melanization. Ascorbate

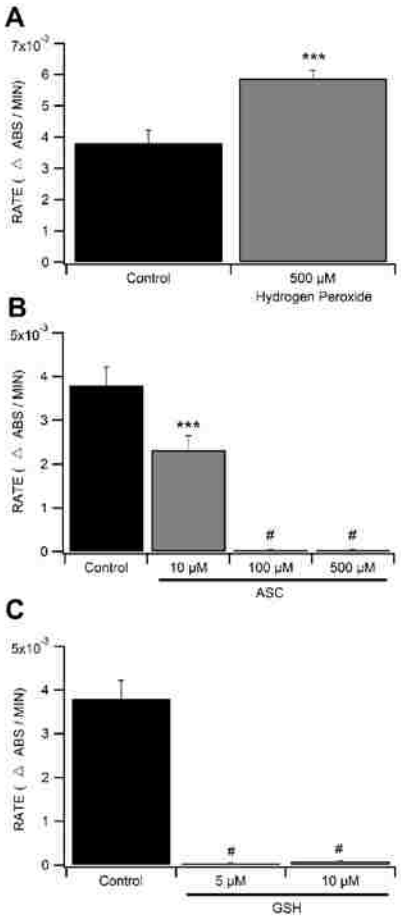

Figure 6. Effect of pro-oxidants and antioxidants on melanin formation. **(A)** Hydrogen peroxide (500 µM) significantly increase DA melanization (30 µM DA) rate (Δ Abs/min). (**B)** Concentration response demonstrating that increased Ascorbic Acid concentrations completely block DA melanization (30 µM DA) rate (Δ Abs/min.). The number of experiments for each condition is n=8 (control), n=4 (10 µM), n=4 (100 µM), and n=4 (500 µM). (**C)** Two low concentrations of GSH that entirely block DA melanization (30 µM DA) rate (Δ Abs/min.). Note that these concentrations are three orders of magnitude lower than those of ASC, and much lower than GSH levels normally seen in cells. The number of experiments for each condition is n=8 (control), n=4 (5 µM), and n=4 (10 µM).

suppressed the formation of melanin at 100 µM or higher (**Fig. 6B**). All concentrations of ASC were shown to be significant when compared against the DA control via one-way ANOVA ($F_{(3,16)}$=36.009, p<0.0001). Individual concentrations showed that 10 µM, 100 µM, and 500 µM ASC were each significant when compared against the non-antioxidant control (respectively, $F_{(1,10)}$=34.297, p<0.001; $F_{(1,10)}$=38.937, p<0.0001; $F_{(1,10)}$=39.226, p<0.0001).

Ascorbate had an approximate IC_{50} of 10 μM. Although there is a trend of decreasing rates with increasing concentrations of ASC, these values are not actually significant from each other as demonstrated by a Tukey post-hoc analysis. GSH had a similar but more efficient action, suppressing DA melanization at concentrations as low as 5 and 10 μM (**Fig. 6C;** respectively, $F(1,10)=38.957$, $p<0.0001$; $F(1,10)=38.771$, $p<0.0001$).

Neuromelanin is found inside DA cells. Since the previous experiments were run in ECF buffer, we validated the highlights (10 μM Fe^{3+} and 5 μM GSH) by replicating them using an ICF buffer (**Fig. 7**). As seen in the figure, trends match those seen with the ECF buffer ($F_{(2,9)}=228.715$, $p<0.0001$).

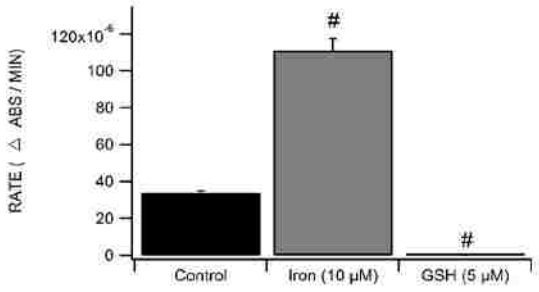

Figure 7. Melanization in intracellular fluid.
Iron (Fe^{3+}) increases the rate of melanization as compared to a control of just DA (30 μM) dissolved in ICF. Reduced glutathione (5 μM), was able to block melanization. This data matches the trends seen in ECF, with pro-oxidants enhancing the rate of melanization and anti-oxidants suppressing the rate of melanization. The number of experiments in each condition is n= 4 (control), n=4 (10 μM iron), and

To confirm the spectrophotometric recordings of the conversion of DA to melanin, we replicated our findings using fast-scan cyclic voltammetry (FSCV). Our voltage ramp was sufficient to measure both the concentration of DA and the concentration of melanin simultaneously. We ran two conditions to confirm our spectrophotometry findings. First, we

added DA into 3 mL of ECF buffer for a resulting concentration of 30 µM and monitored the conversion of DA to melanin over 2 hrs (**Fig. 8A**). Second, we combined GSH (100 µM) with 30 µM DA in ECF buffer (**Fig. 8B**). Under these conditions, our carbon fiber electrodes detected no melanin peak, leading us to conclude that GSH was able to block melanization ($F(1,5)$=10.427, p=0.023). Additionally, we wanted to confirm that DA released from a biological source could melanize under the same conditions. We measured DA release evoked in oxygenated striatal slices following addition of 100 mM KCl to evoke massive DA release from DA terminals. Just as we saw with chemically manufactured DA in our other trials, we observed a DA peak arise early and decay as a melanin peak rose later in the collection (**Fig. 8C**). A direct comparison of the mean rates of melanization show that the trends seen from DA evoked from striatal release are comparable to the trends determined using spectrophotometry (**Fig. 8D**).

3.3 Exposure to Methamphetamine increases Dopamine Release through an Increase of Reactive Oxygen Species

3.3.1 Determine the EC_{50} of Methamphetamine in Slice Preparation in Different Regions of Dopamine Release

Using fast scan cyclic voltammetry (FSCV), we evaluated the effects of METH (0.1 – 100 µM) in the brain slice on two mechanisms of DA release in the NAc core: phasic DA release and DA efflux. Phasic DA release is electrically-evoked with a pulse train of 20 Hz and 10 pulses while DA efflux is independent of any artificial stimulation and occurs only after METH administration. Methamphetamine significantly increased the peak amplitude of the phasic DA signal with an EC_{50} of about 5 µM (**Fig. 9 A-C;** $F_{4,30} = 4.27$, $p < 0.01$). Methamphetamine also

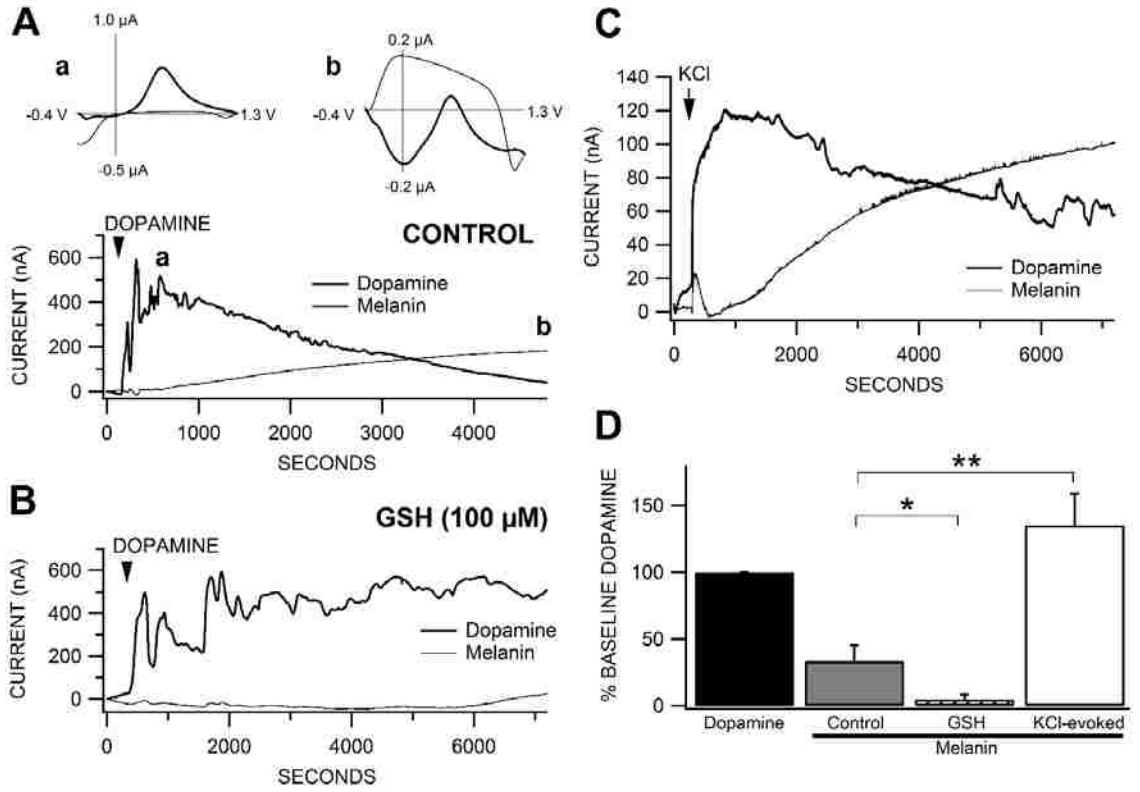

Figure 8. Fast-scan cyclic voltammetry of dopamine melanization.
(A) Insets show representative cyclic voltammograms at the points indicated on the graph during equilibration (Aa) of DA (30 µM) and following partial conversion of DA to melanin (Ab) in a closed system (3 mL of ECF). The characteristic oxidation peak at 0.5 V and reduction peak at -0.38 V are evidence of DA (Aa). The DA redox peaks are still visible (0.5 V and -0.38 V) more than 2 hrs after equilibration (Ab), but significantly reduced, indicating that DA is still in solution, but the redox signal slowly decays as the signal from melanin grows (a broad peak extending from -0.02 V and a sharper peak at -0.4 V). **(B)** In the presence of GSH, melanin does not appear, and the DA signal (30 µM) does not decay. **(C)** Striatal tissue exposed to KCl releases DA. Over time, this DA signal decreases, corresponding with a growing melanin signal. **(D)** Quantitative representation of the representative plots showing the relative concentrations of DA and melanin. The number of experiments for each condition is n=4 (DA), n=4 (control), n=4 (GSH), and n=3 (KCl-evoked).

was able to induce spontaneous (i.e. no artificial stimulation) DA efflux with a similar EC_{50} (**Fig. 9 D-F**; $F_{4,16} = 3.54$, $p < 0.05$).

3.3.2 Methamphetamine Drives Transporter-mediated Dopamine Efflux in the Nucleus Accumbens Independent of Action Potentials or Artificial Stimulation

To better understand the nature of both mechanisms of DA release, we evaluated both in the presence of lidocaine (100 µM), a voltage-gated sodium channel blocker. Lidocaine

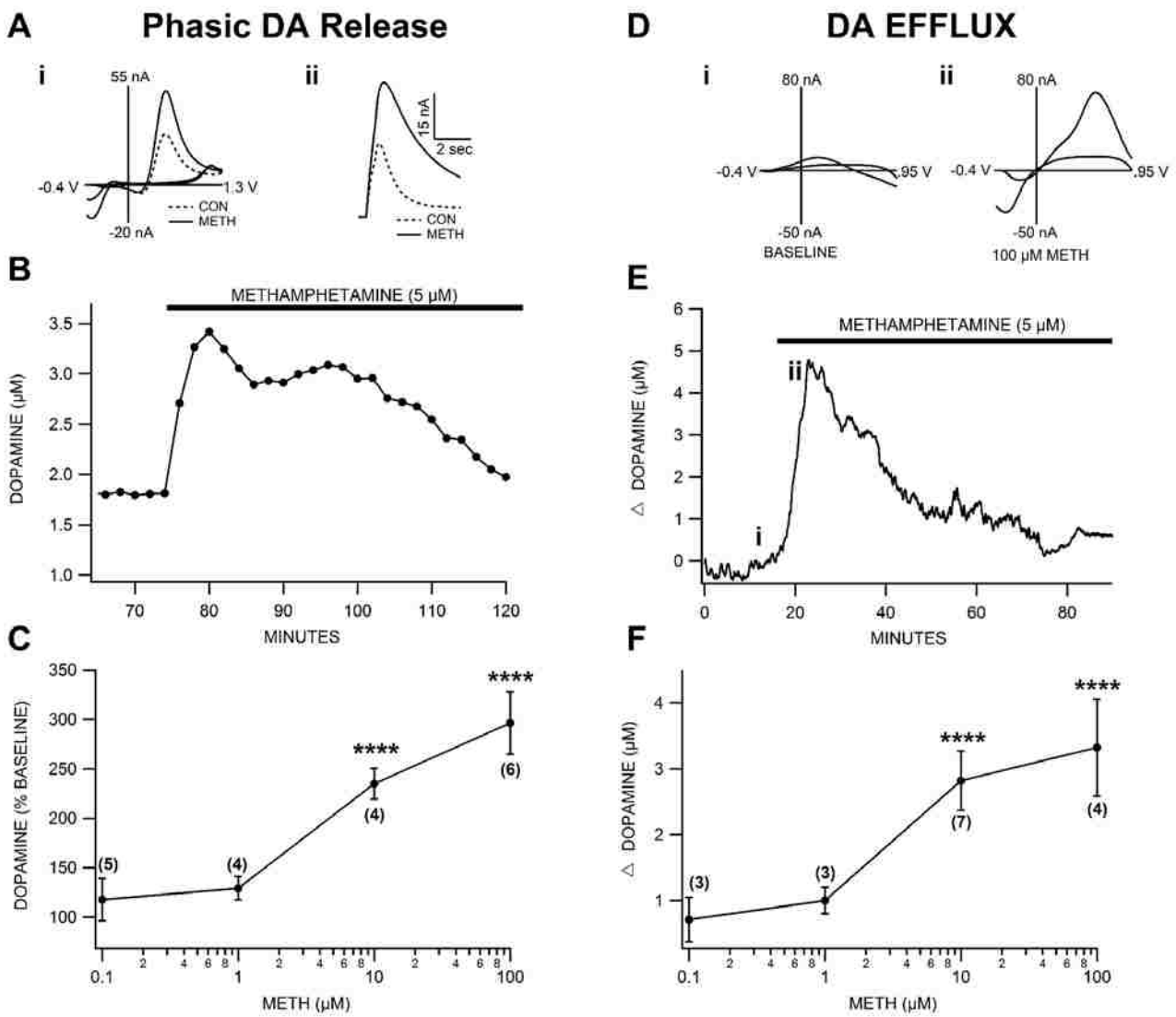

Figure 9. Action-potential dependent DA release (A, B, & C) DA efflux (D, E, & F).
Ai demonstrates a cyclovoltammogram for phasic DA release and **Aii** shows an IvsT plot following local tissue stimulation and the resulting DA spike. **Di** and **Dii** show cyclovoltammograms of a typical DA efflux experiment for before and after METH administration. Representative examples of phasic DA **(B)** and DA efflux **(E)**. Dose-response of METH for phasic DA **(C)** and DA efflux **(F)**. The concentration response experiments showed that METH has the same EC_{50} (~5 µM) for both mechanisms of DA release. Values in parentheses indicate n values.

suppressed phasic DA release (**Fig. 10, A,C-left**; 100 µM lidocaine: $F_{1,16} = 15.04$, $p < 0.001$), while having no impact on DA efflux resulting from acute METH (**Fig 10, B,C-right**; 100 µM lidocaine: $F_{1,10} = 0$, ns). To determine if DA efflux is the same DAT-mediated DA efflux described by others, we analyzed METH-induced DA release in the presence of GBR 12909 (300 nM), a selective DAT blocker. As expected, and similar to METH, GBR 12909 decreased

DA uptake rates (the ratio of $\tau_{after}/\tau_{before}$ for GBR 12909 is 2.76 while for METH it is 7.41). Also, GBR 12909 markedly reduced METH-induced DA efflux (**Fig. 10, E,F-right**; 300 nM GBR 12909: $F_{1,9} = 13.16$, $p < 0.01$), but failed to significantly prevent METH-induced increases in phasic DA release (**Fig. 10, D,F-left**; 1 μM GBR 12909: $F_{1,16} = 1.94$, ns). While two different concentrations of GBR 12909 were used, this does not change the interpretation. Higher concentrations would have more nonspecific targets, specifically serotonin and norepinephrine transporters. However, fluoxetine (a selective SERT blocker) and desipramine (a selective NET blocker) have no effect on DA clearance in the NAc [127, 128]. These experiments confirm that METH-induced DA efflux is DAT mediated (and most likely the same efflux described by others), and that decreases in DAT function mediate the METH-induced increases in phasic DA release [80, 129].

3.3.3 Determine if Methamphetamine Increases Reactive Oxygen Species Generation and Where this Happens Anatomically

To determine ROS production in the NAc following chronic METH self-administration, we carried out immunohistochemical experiments with an antibody against 8-hydroxyquanine (8-OHG) antibody (Abcam, ab62623), a cellular marker of oxidative stress [130, 131]. Methamphetamine self-administering rats showed a significant increase in numbers of 8-OHG positive cells about two-fold as compared with controls (**Fig. 11, C**; Student's *t*-test, $P < 0.05$ vs. controls, $n = 3$-4). To further identify the types of cells producing ROS, we performed double immunofluorescence labeling using cell type markers: NeuN (a marker for neuron; green); GFAP (a marker for astrocytes; green); Iba-1 (a marker for microglia; green); and NG2 (a marker for oligodentrocytes; green). These results demonstrated that most 8-OHG positive cells (red signal) were co-localized with NeuN-positive neurons in the NAc (green nucleus with red

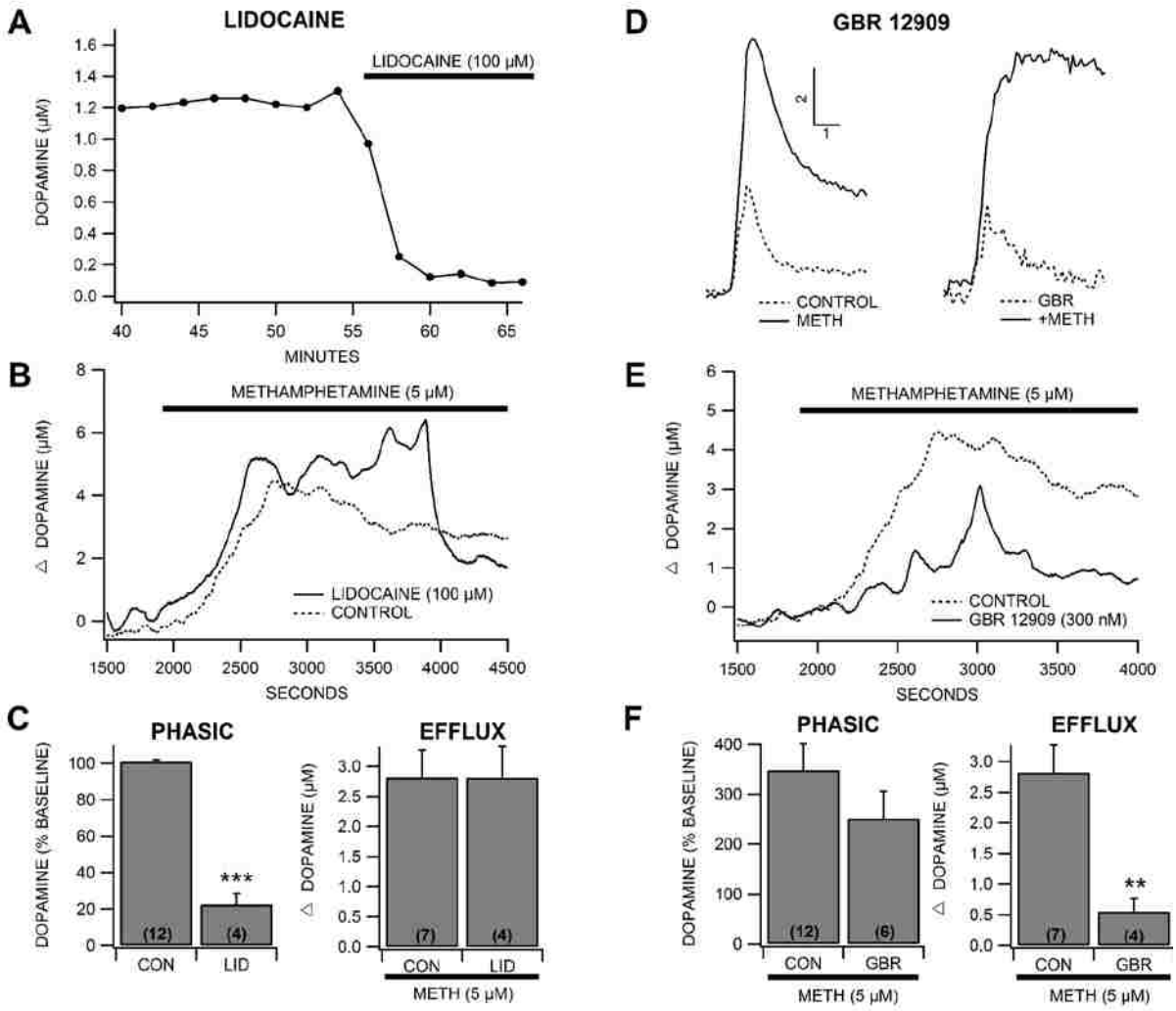

Figure 10. Lidocaine and GBR 12909 block phasic dopamine release without having an effect on dopamine efflux.

Phasic DA release was completely abolished by lidocaine (100 µM) (**A, C-left**). Cumulative phasic data is expressed as a percent change, but averaged raw values are: Control = 1.28 ± 0.52 µM, Lidocaine = 0.20 ± 0.05. Since we were unable to measure DA efflux without METH being present to drive it, we tested lidocaine (100 µM) against METH (5 µM) (**B,C-right**). A quantitative analysis showed that while METH was unable to decrease METH-induced efflux, it significantly inhibited electrically-evoked DA release. This suggests that phasic DA release is dependent upon action potentials, while METH-induced DA efflux is independent, likely being driven by an intracellular process or event. GBR 12909 (1 µM), a DAT inhibitor, fails to attenuate METH-enhancement of electrically-evoked DA release (**D,F-left**). Averaged raw phasic values are: control baseline = 0.57 ± 0.15 µM; control METH = 1.52 ± 0.32 µM; experimental baseline = 0.84 ± 0.27 µM; GBR 12909+METH = 1.48 ± 0.32 µM. GBR 12909 (300 nM) blocked METH-induced DA efflux (**E,F-right**). ** $p<0.01$ and *** $p<0.001$ as compared to control values. Values in parentheses indicate n values.

circle in **Fig. 11F**), but not astrocytes, microglia or oligodendrocyte (**Fig. 11, I,L, and O)**. These data indicate that increased ROS production in the NAc of rats self-administering METH occurs

mostly in neurons.

3.3.4 The Sigma Receptor is involved in Methamphetamine's Mechanism of Enhancing Dopamine Release

Methamphetamine is a potent agonist of σ1Rs [132, 133]. Also, in cultured neurons, blocking the σ1R prevents METH-induced formation of ROS and DA release [98]. To extent these studies in cultured cells, the σ1R selective antagonist BD 1063 was pre-applied to prevent METH-σ1R interactions. BD 1063 prevented METH enhancement of both phasic DA release (**Fig. 12, A,C-left**; 1 μM BD 1063: $F_{1,16} = 4.96$, $p < 0.05$) and METH-driven DA efflux (**Fig. 12, B,C-right**; 100 nM BD 1063: $F_{1,9} = 12.97$, $p < 0.01$). σ1R activation is thought to increase ROS production by increasing intracellular Ca^{2+} signaling [134]. Therefore, Ca^{2+} stores were depleted using the ER Ca^{2+} ATPase inhibitor cyclopiazonic acid (CPA, 10 μM), and METH-induced DA release was measured. CPA significantly attenuated METH's effect on both DA efflux (**Fig. 12, E,F-right**; 10 μM CPA: $F_{1,9} = 11.30$, $p < 0.01$) and phasic release (**Fig. 12, D,F-left**; 10 μM CPA: $F_{1,16} = 5.062$, $p < 0.05$).

3.3.5 Determine if Antioxidants are able to block Methamphetamine's Enhancement of Dopamine Release

Methamphetamine increases oxidative stress [135-137]. While it is known that oxidative stress is a result of excess DA, we sought to determine if oxidative stress affects DA release. One report has shown that overexpression of superoxide dismutase blocks METH-induced DA depletion in cultured neurons [135], indicating that there may be ROS formation before METH changes DA concentrations. In slice voltammetry experiments, we tested whether the superoxide scavenger TEMPOL could block the acute effects of METH (5 μM) on DA release. TEMPOL

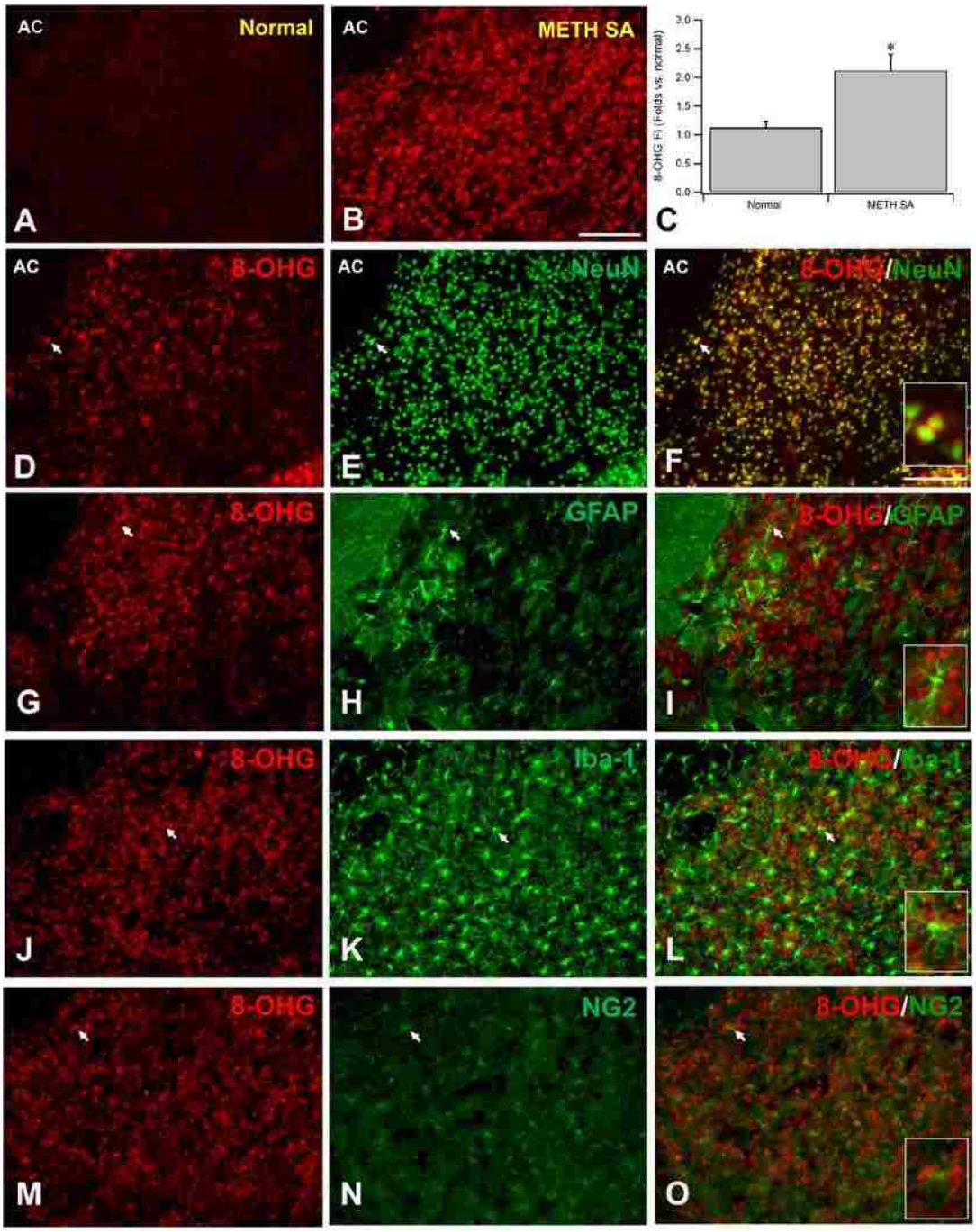

Figure 11. Increased oxidative stress in neurons of the nucleus accumbens in rats self-administering methamphetamine (METH).

A, B: Immunohistochemical staining of 8-hydroxyguanine (8-OHG; red), an oxidative stress marker, in the NAc of normal (Normal; A) or METH self-administering (METH SA; B) rats. **C:** A significant increase in fluorescence intensity of 8-OHG (8-OHG FI on y-axis) was found in the NAc of METH SA rats (C), compared to that of controls (A; * $P < 0.05$). **D-O:** These images show double-immunostaining in the NAc for 8-OHG (red) with NeuN (neurons; green) and merge (F), GFAP (astrocytes; green) with merge I, Iba-1 (microglia; green) with merge L, and NG2 (oligodendrocytes; green) with merge O. Most 8-OHG positive cells were double-labeled with NeuN (F). Note double-labeled cells of green nucleus (NeuN) surrounded by red cytoplasm (8-OHG) in neurons (F), but not other cells (I, L, O). AC= anterior commissure. n = 3 - 4 per group. *Scale bar* = 50 µm.

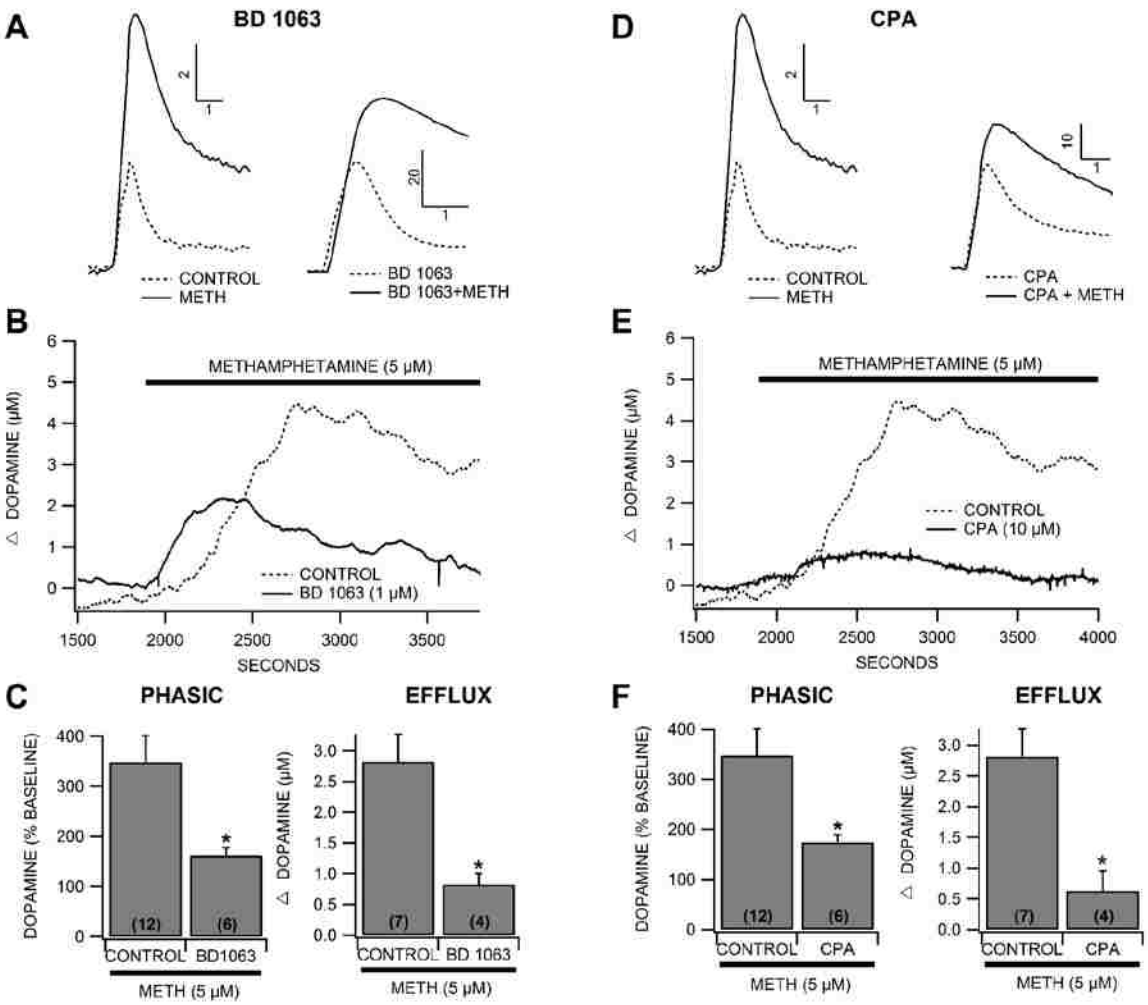

Figure 12. The sigma receptor antagonist BD 1063 induces a partial block of methamphetamine-induced dopamine release.

The increase of phasic DA caused by METH is not as intense in the presence of BD 1063 (1 µM) (**A**). Similarly, METH-induced efflux shows much lower DA release in the presence of BD 1063 (1 µM) (**B**). A quantitative representation of both efflux and phasic DA release (**C**). Averaged raw phasic values for BD 1063 are: control baseline = 0.57 ± 0.15 µM; control METH = 1.52 ± 0.32 µM; experimental baseline = 0.97 ± 0.31 µM; CPA+METH = 1.59 ± 0.58 µM. Cyclopiazonic acid (10 µM), which depletes intracellular Ca^{2+} stores, decreases METH enhancement of both phasic DA release (**D,F-left**) and DA efflux (**E,F-right**). * p <0.05 as compared to control values. Averaged raw phasic values for CPA are: control baseline = 0.57 ± 0.15 µM; control METH = 1.52 ± 0.32 µM; experimental baseline = 0.82 ± 0.24 µM; CPA+METH = 1.33 ± 0.32 µM. Values in parentheses indicate n values.

attenuated METH-induced enhancement of phasic DA release (**Fig. 13, A,C-left**; 1 mM TEMPOL: $F_{1,17} = 5.51$, $p < 0.05$), and decreased METH-evoked DA efflux (**Fig. 13, B,C-right**; 1 mM TEMPOL: $F_{1,10} = 5.34$, $p < 0.05$), suggesting that ROS production is necessary for some of METH's effects on DA release.

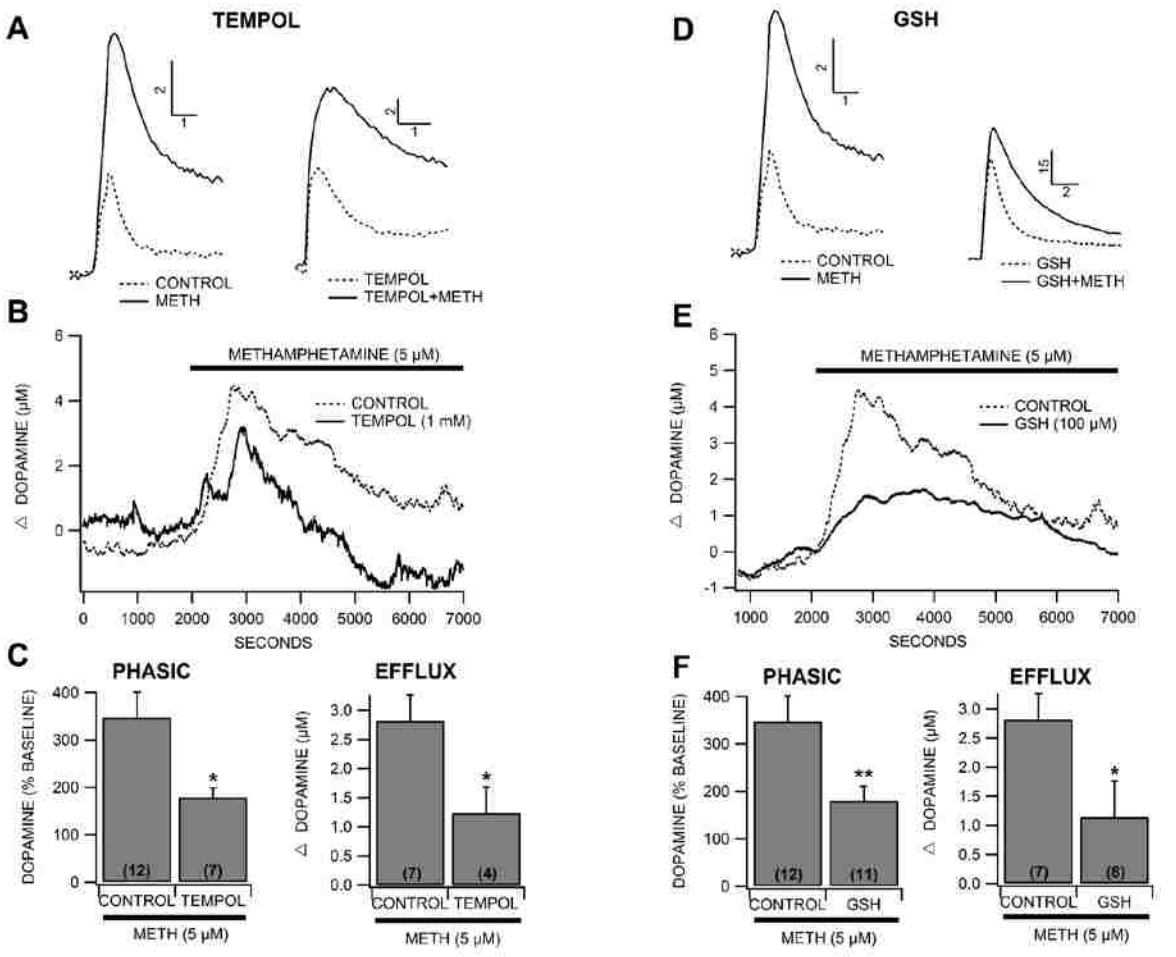

Figure 13. Effects of antioxidants.
TEMPOL (a SOD-mimetic) is able to partially block the transient phasic increases of DA release (**A**) as well as METH-induced DA efflux (**B**). Glutathione (the substrate for glutathione peroxidase, an enzyme that decreases levels of hydrogen peroxide) is able to partially block METH-induced increases of phasic DA (**D**) as well as METH-induced DA efflux (**E**). Quantitative analyses show these trends for both TEMPOL and GSH (**C, F**). Averaged raw phasic values for TEMPOL are: control baseline = 0.57 ± 0.15 μM; control METH = 1.52 ± 0.32 μM; experimental baseline = 0.53 ± 0.08 μM; TEMPOL+METH = 0.99 ± 0.10 μM. Averaged raw phasic values for GSH are: control baseline = 0.57 ± 0.15 μM; control METH = 1.52 ± 0.32 μM; experimental baseline = 1.38 ± 0.30 μM; GSH+METH = 2.24 ± 0.53 μM. * $p < 0.05$ as compared to control values. Values in parentheses indicate n values.

To elaborate on the role of pro-oxidants, we examined an antioxidant system endemic in cells: glutathione peroxidase (GPx). Specifically, we tested the effects of reduced glutathione (GSH), a substrate for GPx, an endogenous ROS scavenger, on METH-induced DA release. GSH (100 μM) attenuated METH enhancement of DA release, both phasic release (**Fig. 13, D,F-left**; 100 μM GSH: $F_{1,25} = 9.87$, $p < 0.01$) and the DA efflux (**Fig. 13, E,F-right**; 100 μM GSH: $F_{1,13}$

= 6.92, $p < 0.05$), further confirming that endogenous ROS production is involved in METH's effects on DA release.

3.3.6 Reactive Oxidative Species causes S-glutathionylation of VMAT2, Impairing Function

Methamphetamine-induced DA efflux can be blocked by tetrabenazine, a VMAT blocker [138]. While this could be partly due to METH's effects on the VMAT [82], METH-induced ROS production may also be altering VMAT. Therefore, we tested whether directly increasing ROS production can induce changes in VMAT function through protein modification. Recombinant human VMAT protein was isolated and exposed to disulfiram (to induce S-glutathionylation) and subsequently analyzed using mass spectrometry. These studies revealed that Cys 488 became S-glutathionylated in the presence of disulfiram (**Fig. 14**). This post-translational modification proved to dramatically decrease VMAT2 function in an activity assay using protein purified from fresh mouse accumbens tissue (**Fig. 15**; $F_{1,6} = 576.96$, $p < 0.001$).

3.3.7 Parallel Mechanism in the Nucleus Accumbens Shell

Since the NAc core and shell have different roles, we determined the effects of METH on DA efflux in the NAc shell to compare with our results in the core. Methamphetamine (5 μM) induced DA efflux in the shell. While not significantly different from efflux in the core, it appears that the shell may be slightly less sensitive than the core (**Fig. 16**; $F_{1,11} = 3.74$, $p = 0.079$). Additionally, we determined that BD 1063 (100 nM) is able to attenuate the effects of METH (5 μM) in the NAc shell (**Fig. 16**; 100 nM BD 1063: $F_{1,8} = 9.77$, $p < 0.05$).

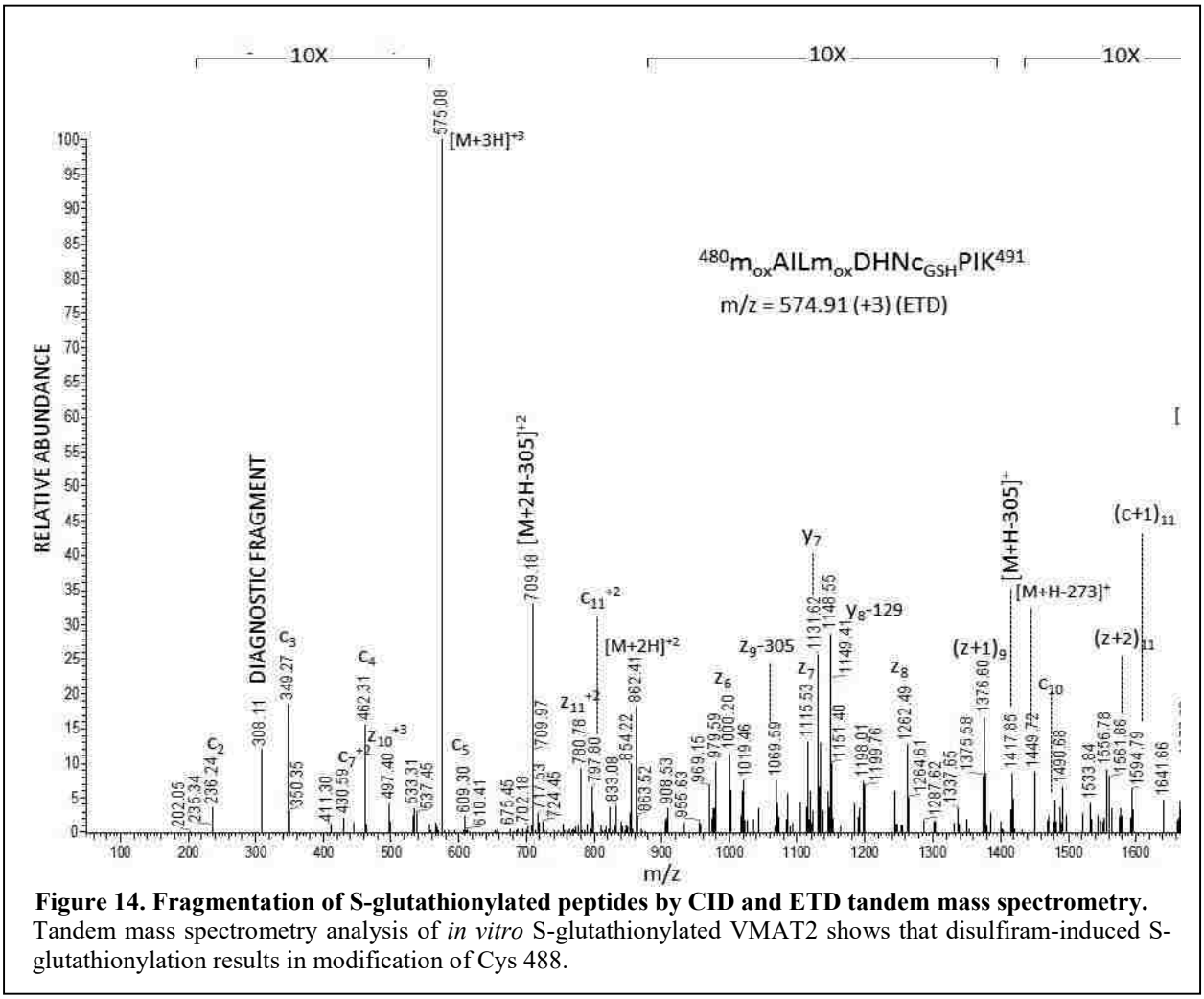

Figure 14. Fragmentation of S-glutathionylated peptides by CID and ETD tandem mass spectrometry. Tandem mass spectrometry analysis of *in vitro* S-glutathionylated VMAT2 shows that disulfiram-induced S-glutathionylation results in modification of Cys 488.

3.3.8 Acute Methamphetamine Causes S-glutathionylation of VMAT2 and Increases Oxidative Stress in the Nucleus Accumbens

Using an antibody against 8-hydroxyguanosine (8-OHG, a mutated nucleic acid formed by exposing DNA to oxidative stress), we quantified relative levels of oxidative stress in animals following acute IP drug administration. Methamphetamine (5 g/kg) increased levels of 8-OHG as compared with saline-injected controls (**Fig. 17, A-C**; $F_{1,25} = 8.17$, $p < 0.01$).

Although VMAT2 function was inhibited by METH *in vitro*, we were interested to see if *in vivo* administration of METH (IP, 10 mg/kg) might affect VMAT2 function through S-

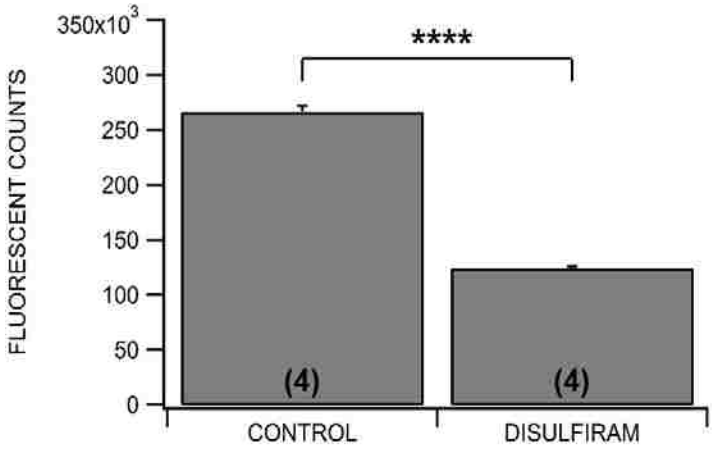

Figure 16. S-glutathionylations in the nucleus accumbens decreases VMAT2 activity.
C57BL/6 accumbens tissue was S-glutathionylated *ex vivo* with 10 µM disulfiram followed by measurement of VMAT2 activity with 4-(2-Aminoethyl)-7-(methylamino)-2H-chromen-2-one trifluoroacetate. $p<0.0001$. Protein samples exposed to disulfiram displayed a greatly reduced activity as compared to matched control samples. This indicates that the S-glutathionylation modification of cysteine residues decreases VMAT2 function. **** $p<0.0001$ as compared to the controls. Values in parentheses indicate n values.

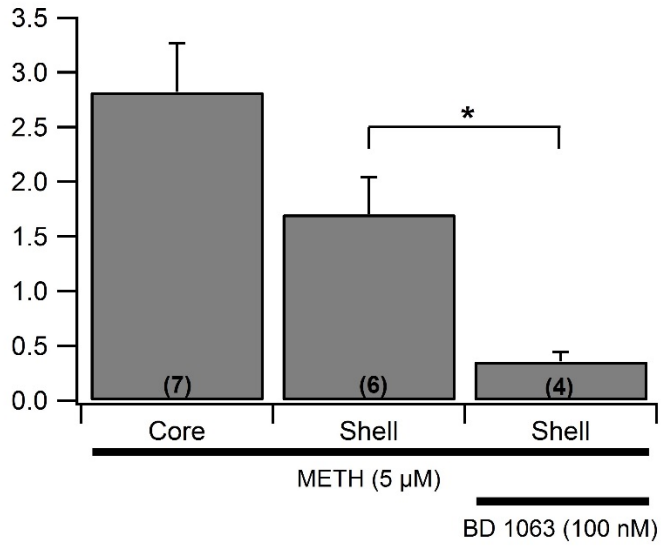

Figure 15. Methamphetamine effects in the nucleus accumbens shell.
Methamphetamine induced dopamine efflux occurs in both the nucleus accumbens core and shell. Although there appears to be a trend for decreased sensitivity in the shell, this is not significant. The effects of METH are blocked by BD 1063 in the shell, indicating that the outlined mechanism of METH-induced dopamine release is the same as in the core. *$p<0.05$ as compared against the shell controls. Values in parentheses indicate n values.

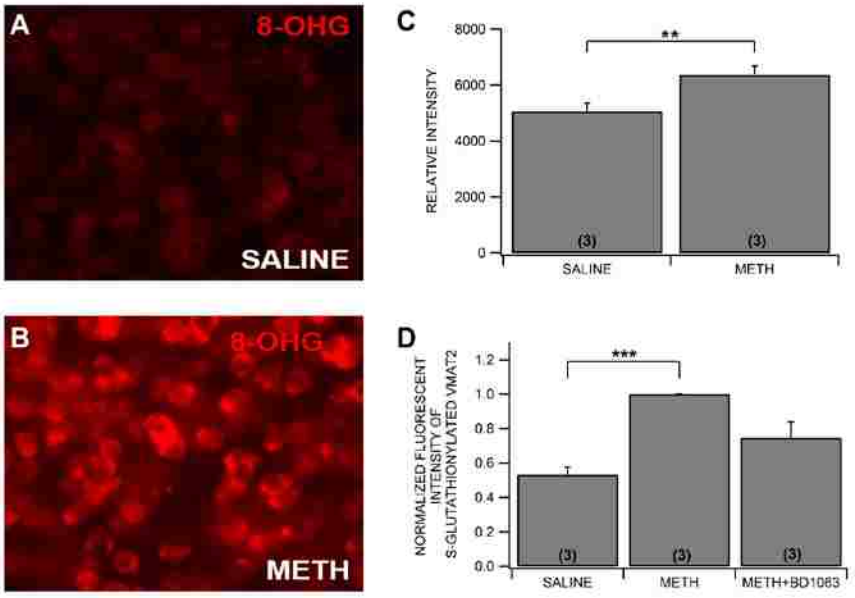

Figure 17. S-glutathionlyation of VMAT2 and enhancement of oxidative stress after acute methamphetmaine.
(A) 8-OHG stain in NAc core in vehicle-injected (saline) animals. (**B**) 8-OHG stain in NAc core in METH-injected animals. (**C**) Immunohistochemical staining for 8-OHG, a marker of oxidative stress. Oxidative stress increased following an injection of acute METH as compared with a control saline injection. (**D**) Fluorescent intensities for S-glutathionylated VMAT2 normalized against total VMAT2 intensity (n=3). Animals injected with METH show increased levels of S-glutathionylation as compared with controls and BD 1063 reduces METH enhancement of S-glutathionylation. Asterisks **,*** represent significance level $p < 0.01$ and $p < 0.001$, respectively. Values in parentheses indicate n values.

glutathionylation and if BD 1063 (IP, 30 mg/kg) could prevent it. Using a co-immunoprecipitation assay, administration of 10 mg/kg IP METH increased levels of modified VMAT2 as compared with saline controls (**Fig. 17, D**; $F_{1,4} = 112.06$, $p < 0.001$). BD 1063 appeared to decrease METH's ability to modify VMAT2, albeit not quite significantly (**Fig. 17, D**; $F_{1,4} = 7.64$, $p = 0.051$).

4 DISCUSSION

4.1 Conversion of Dopamine to Melanin

Dopamine spontaneously polymerizes into melanin, with the rate of formation being highly dependent on initial DA concentration. While DA metabolic precursors and metabolites also can form into melanin, DA possesses unique chemical attributes that allow it to melanize more rapidly than related compounds. Following our initial investigations of melanization, we followed two parallel hypotheses for how the rate of melanization can be maximized. The first hypothesis focused on the possible role of the catechol functional group of DA-coordinating cations, specifically Fe^{3+} and Ca^{2+} as both these ions are able to associate with catechol groups [139]. The second line of investigation focused on a radical hypothesis, in which melanin is a polymer made of covalently bound DA molecules. The process of polymerization would involve a radical intermediate.

4.1.1 The Cation Hypothesis of Melanization

Iron (III) increased the rate of melanization (EC_{50} = 50 nM). However, Fe^{3+} can be implicated in both the cation (via catechol binding) and the radical (by generating radicals via the Fenton reaction) hypotheses. In order to help us elucidate the differences between the cation hypothesis and the radical hypothesis, we determined whether another cation has a similar ability to induce melanization. A key ion to examine with was Ca^{2+}: It is biologically

relevant in varying concentrations and, like Fe^{3+}, is known to associate with catechol groups [139]. Additionally, a key difference between DA cells in the VTA vs. SNc is that VTA DA cells have less intracellular Ca^{2+} than do SNc DA cells [140], meaning that increased Ca^{2+} correlates with NM deposits, implicating a possible role for Ca^{2+} with *in vivo* NM formation. Despite previous evidence for Ca^{2+} driving some form of melanization[141], our results showed that once iron contamination was removed from the calcium salts, Ca^{2+} was unable to drive melanization within the time range studied. Based on these results, we largely reject the cation hypothesis of DA melanization. However, because of the large increase in polymerization when 10 μM Fe^{3+} was the catalyst, we cannot fully reject this theory. 10 μM Fe^{3+} provides the ideal stoichiometry for maximum aggregation of DA molecules around one Fe^{3+} (3 DA: 1 Fe^{3+}). Each DA molecule has one catechol with two hydroxyl groups each providing lone electron pairs that can corm coordinate covalent bonds to Fe^{3+}, which has six coordination sites.

4.1.2 The Radical Hypothesis of Melanization

We pursued the idea that melanization was partially dependent on reactive oxygen species (ROS) or on radical intermediates. As mentioned earlier, the enhanced rate of melanization by Fe^{3+} can be easily explained either by Fe^{3+} interacting with DA's catechol or by iron's ability to exchange electrons. Iron is able to induce lipid peroxidation and catalyze the formation of superoxide (21,35). If free radicals from iron enhance melanization, then a free radical from H_2O_2 should also be able to catalyze the reaction of DA into melanin. It has already been shown by Zecca et al., that a high concentration of H_2O_2 (approximately 1 M) is able to degrade NM [74], so we analyzed a much smaller concentration of H_2O_2 (500 μM). The results clearly demonstrated (**Fig. 6A**) that this concentration of H_2O_2 enhance melanization. We thus conclude that DA neurons are able to buffer small amounts of H_2O_2-

related oxidative stress, but that under chronic conditions of high levels of H_2O_2 this natural ROS buffer is overwhelmed and degrades.

Simply adding H_2O_2 is not enough to confirm that the presence of ROS can drive melanization, as H_2O_2 is particularly volatile and decomposes quickly. Because of this, measuring accurate concentrations of H_2O_2 is difficult under reaction conditions. However, antioxidants are very stable in solution and are easy to measure accurately. Thus, we investigated the effect of antioxidants on the rate of melanization. The first logical choice of antioxidant was ascorbate (ASC). Ascorbate is found across the brain in varying quantities dependent on anatomical location. In particular, ASC is found in low millimolar levels in the striatum and at least an order of magnitude lower in the midbrain tegmentum where DA neurons originate [142]. Higher concentrations of ASC (1-5 mM) were able to completely block melanization. This may explain why NM forms in cell bodies (tegmentum), but not in terminal areas (striatum). Our experiments had shown that whenever we kept DA in solution, it would spontaneously turn into melanin, so why doesn't DA spontaneously form into NM in the striatum? We speculate that the combination of high concentrations of ASC and low concentrations of iron in the striatum might prevent melanization.

Ascorbate is not the only antioxidant endemic to the DA system. Glutathione oxidation has been heavily implicated in DA cell health [143]. This relationship between melanin growth and oxidative stress is interesting. In the brain, DAergic neurons are particularly susceptible to oxidative stress. In fact, DAergic neurons require a higher baseline level of GSH (35±3 nmol/mg in DAergic cells as compared to 8±0.4 nmol/mg) for normal function [144]. Dopamine levels drop an additional 30-40% as PD progresses without a corresponding increase of oxidized GSH (GSSG) [145]. This is peculiar considering that the SNc has relatively high

concentrations of iron deposits [70, 146], which should increase oxidative stress in this area of the brain. Additionally, DA metabolites (notably H_2O_2 and DOPAL) are also ROS.

Taking this into consideration, we propose a model for DA melanization (**Fig. 18**). In this model, we speculate that DA molecules aggregate around a Fe^{3+} ion. Once in close proximity, it is possible for radicals to travel between the molecules, creating covalent bonds. This polymerization continues, creating chains of covalently linked DA molecules (in varying states of oxidation).

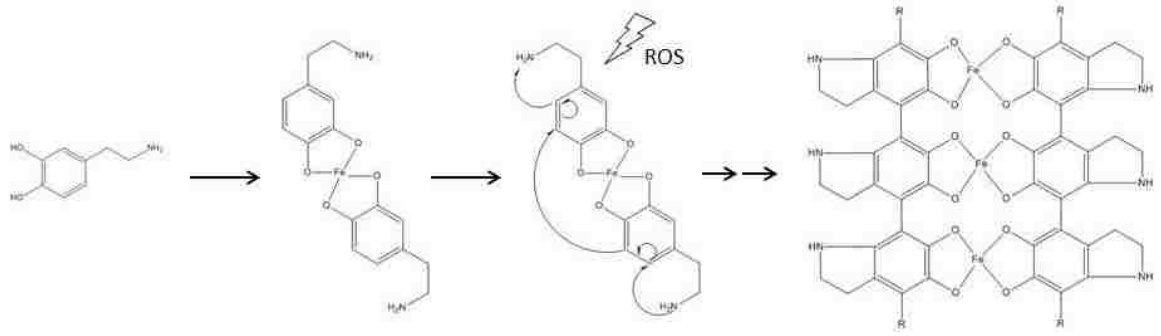

Figure 18. Proposed model for dopamine melanization.
To get optimal formation of melanin, two factors are necessary: chelation and radical polymerization. Dopamine molecules chelate iron by the catechol group, positioning the DA molecules to allow for quick radical polymerization between the benzene rings in response to ROS. Although only two DA molecules are shown coordinating the iron atom, there are most likely three DA molecules as there are six coordination sites on the iron.

Although previously thought otherwise, a growing body of literature is identifying NM as a neuroprotective polymer [74], likely due to nascent antioxidant properties. For example, in models of PD, cells containing less NM are more susceptible to death [64, 65]. We propose that DA neurons use NM as a mechanism to deal with this oxidative stress. We suggest that NM may be able to act, at least indirectly, as a radical scavenger, decreasing oxidative stress in already over-stressed DAergic cells [74]. Dopamine neurons uniquely manufacture DA, and seem to capitalize on its distinctive chemistry—particularly its ability to spontaneously form

into melanin. Iron bound up in NM may be redox-inactive [75, 147, 148], thus unable to catalyze the Fenton reaction, curtailing production of hydroxyl radicals. Furthermore, DA molecules bound up in NM are likewise unable to be converted by MAO into DOPAL and peroxides. Effectively, we propose that NM is formed in DA somata in response to both oxidative stress and cellular stress (high iron levels). The formation of NM reduces levels of redox-active iron and likely inactivates radicals in the form of peroxides and superoxides. Thus, the presence of NM can be used as a marker of past oxidative or cellular stress. Furthermore, since NM possesses a stable radical [149], it can be an active antioxidant once formed. We further propose that in PD, NM+ cells begin to die when iron levels or oxidative stress exceed the cell's ability to produce NM, or when iron levels overwhelm NM binding sites, as has been previously suggested [67]. In these instances, DA cells are unable to cope with high levels of ROS and succumb quickly to oxidative stress, as natural methods of quenching ROS are compromised as PD progresses [67, 150, 151].

4.2 Methamphetamine's Effects on Dopamine Release

Methamphetamine robustly enhanced both action potential-dependent and independent DA release with an EC_{50} of 5 μM. Lidocaine (100 μM) blocked phasic (electrically evoked, 20 Hz and 10 P) DA release at lower levels than others have reported [152], while leaving METH's effect on the DA efflux unaltered. Lidocaine, a voltage-gated sodium channel blocker, prevents action potential dependent DA release, but not the METH-evoked DA efflux, indicating that the mechanisms underlying electrically evoked and non-evoked release are different. Similar to that shown in previous studies, METH-induced DA efflux is independent of action potentials, but thought to be dependent on DA reverse transport through the DAT [129]. Phasic DA release in the NAc is associated with burst firing activity of DA neurons in the VTA [153]. It has been postulated

that this burst firing and subsequent phasic DA release is critical for proper learning and goal-oriented behavior [154]. Amphetamines increase the potential for learning and goal-oriented behavior [155, 156], indicating that amphetamines may increase phasic DA activity. Indeed, Ingram et al (2002) demonstrated that amphetamines could increase neuronal excitability through increases in DAT-mediated currents [157]. Our results are consistent with previous reports, that METH enhances phasic DA release, most likely through decreases in uptake [80], but can also trigger DA efflux independent of electrical impulses from the cell body [89, 158]. Importantly, increases in extracellular DA tone can influence the ability of the cell to generate phasic responses, specifically through decreases in readily releasable pools, and D2R autoreceptor-mediated inhibition.

4.2.1 Role of the Sigma Receptor in Methamphetamine-induced Production of Reactive Oxygen Species

The σ1R was originally thought to be an opioid receptor as the opioid dextromethorphan was a potent ligand at this receptor. However, this was soon shown to be due to a non-specific drug interaction, and it was discovered that sigma activity was not blocked by the non-selective opioid receptor antagonist naloxone, and that many non-opioids, including METH and cocaine, are also potent σ1R agonists [159]. While this unique receptor is ligand-activated, it is fundamentally different from classic ligand-activated receptors such as GPCRs and ion channels, in that it acts primarily as a chaperone receptor [160]. The σ1R is found on the ER, mitochondria, and on the plasma membrane interfaces [161, 162]. The σ1R has been shown to modulate Ca^{2+} flux at the interface between the ER and the mitochondria [163], and blocking the σR prevents ROS production [98]. Indeed, several reports have shown that both the σ1R and σ2R help regulate the cell's antioxidant potential [164-166] (for complete review, see Katz review [94]). Interestingly,

AC927 (0.3 μM), a σR antagonist with high affinity for both σ1R and σ2R (σ-1R K_i = 30 ± 2 nM, σ-2R K_i = 138 ± 18 nM; [167]), was able to block ROS generation by METH in cultured neurons [98]. Since METH has been shown to increase cytosolic Ca^{2+}, changing the intracellular Ca^{2+} and forming ROS [168], we postulated that increases in cytosolic Ca^{2+} and subsequent ROS formation were initiated upon METH-induced activation of σ1Rs. Indeed, our results confirm that the σR is involved in METH-induced changes in living striatal tissue and functional DA terminal physiology. Also, we were able to show that METH affected two very different types of DA release: synaptic/vesicular (modeled by electrically evoked phasic release) and DAT-mediated efflux through the σR. And while BD 1063 can antagonize both the σ1Rs and σ2Rs, it binds preferentially to the σ1R (K_i = 9 ± 1 nM vs. K_i = 449 nM for σ1R and σ2R, respectively), suggesting that METH's effects on DA release are primarily through σ1R activation, although it is also possible that σ2R activation is involved. Furthermore, depleting intracellular Ca^{2+} levels with CPA (10 μM) prevented METH-induced DA efflux. Since Ca^{2+} is the likely signal between the σ1R on the ER and the mitochondria (for review of Ca^{2+} and the mitochondria, see Contreras et al [169]), it is logical to conclude that this is the mechanism between σ1R activation and ROS formation following METH exposure. Calcium signaling from the endoplasmic reticulum is potentially mediated through inositol 1,4,5-triphosphate (IP_3) levels, as has been suggested by others [170-173].

4.2.2 Methamphetamine-induced Production of Reactive Oxygen Species

Methamphetamine induces oxidative stress in neural tissue. Levels of GSH peroxidase enzymes are lower following exposure to METH in DA cell culture [174], and levels of malondialdehyde, a product of lipid peroxidation, greatly increase in the brain following METH administration [175]. Also, recovering METH addicts evince higher levels of oxidative stress [176].

While it has generally been assumed that most of the oxidative stress associated with METH abuse results from high levels of extra-vesicular DA that is then oxidized and broken down (a byproduct of monoamine oxidase is hydrogen peroxide), this doesn't appear to be the sole source of oxidative stress in DA terminals following METH. Methamphetamine is known to inhibit complexes I, II, III, and IV in the electron transport chain in the mitochondria (for complete review see Barbosa et al, 2015 [177]), indicating that there are other potential sources of oxidative stress. Additionally, since we show that inhibiting both superoxide (TEMPOL experiments) and hydrogen peroxide (GSH experiments) decreases METH-induced DA release, suggesting that there is a secondary source of oxidative stress from METH that occurs upstream to DA vesicular leakage and subsequent auto-oxidation. Further evidence for a direct interaction between METH and mitochondrial-induced ROS formation come from studies where TEMPOL, a membrane-permeable radical scavenger, reduced hydrogen peroxide-mediated decrease in mitochondrial function and malondialdehyde level *in vitro* and *in vivo* [178]. Others have also shown that TEMPOL attenuates mitochondrial-induced oxidative damage by METH and METH-induced sensitization [179]. Based on the results from part 1 of this study, it is likely that the ROS generated by acute METH will lead to melanin formation in DA cells.

4.2.3 Methamphetamine-induced Oxidative Stress and VMAT2

Methamphetamine-initiated widespread oxidative stress is fairly well-known, however, the mechanisms involved are still being elucidated. Chronic oxidative stress from METH exposure is thought to contribute to its neurotoxic effects [180]. However, immediate targets and consequences of the ROS are not well known. ROS can lead to S-glutathionylation, a post-translational modification on cysteine residues within redox sensitive proteins that could lead to a change in structure and function of the target protein [181]. We have shown here using high

resolution mass spectrometry that *ex vivo* disulfiram-induced S-glutathionylation [182] causes modification on Cys 488 of VMAT2. This S-glutathionylation decreases VMAT2 functionality. Decreased VMAT function would prevent vesicles from maintaining "normal" DA concentrations, resulting in DA leakage [129], whether it be through inherently leaky vesicles [183] or through a disrupted proton gradient [184]. Decreased VMAT function will result in DA accumulation in the synapse, and eventual efflux through the DAT, as well as intracellular metabolization of DA via mitochondria-associated monoamine oxidases. Buildup and breakdown of DA increase oxidative stress (both inside and outside of the cell), as DA metabolites include superoxide, hydrogen peroxide, DA quinones, and 3,4-dihydroxyphenylacetaldehyde (DOPAL) [185-187]. This adds to METH-induced neurotoxicity. Supporting these findings, it has been shown that increasing expression of VMAT2 will help protect against METH neurotoxicity [188] and that chronic METH users show decrease VMAT2 expression [189]. The present study shows that application of strong antioxidants, such as TEMPOL, is sufficient for blocking METH's effects on DA efflux.

4.2.4 Mechanistic Model of Methamphetamine-induced Dopamine Release

The current mechanistic model behind METH's increase of DA release states that METH enters the DA terminal through DAT. Once in the cytosol, METH inhibits VMAT2, blocking vesicle transport and inducing vesicle depletion. The accumulation of DA in the cytosol overpowers the DAT, causing reverse transport. The current study adds considerable detail to the intracellular actions of METH. Once METH is inside the cell, it appears to activate the σ1R, altering proper Ca^{2+} signaling between the smooth ER and the mitochondria, resulting in disrupted mitochondrial function, and causing superoxide production. Superoxide (mechanistically related to many other ROS [190]) then causes S-glutathionylation of VMAT2,

which prevents proper function of VMAT, allowing for DA-containing vesicles to be depleted. The DA released from vesicle pools flows out through the compromised DAT. For illustration, see figure 19.

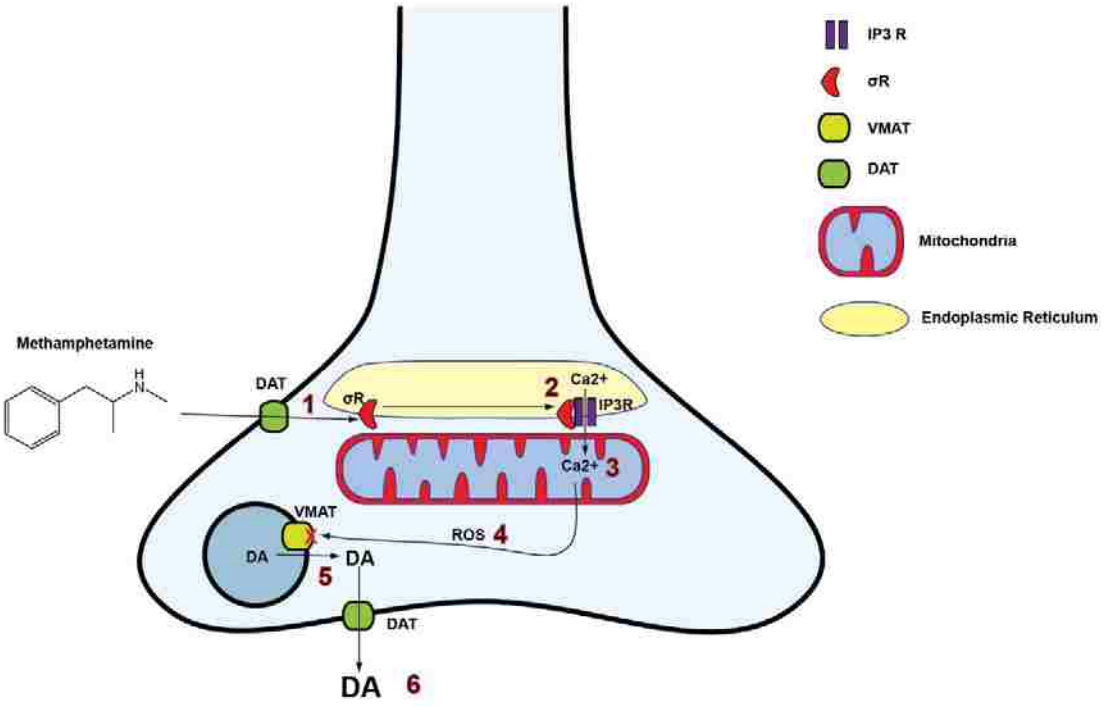

Figure 19. Model of Methamphetamine-induced Dopamine Efflux.
1. Methamphetamine enters DA terminals through the DAT. 2. Methamphetamine activates σ1Rs on the endoplasmic reticulum, resulting in σ1R activation of Ca^{2+} signaling, potentially through the IP_3R. 3. Ca^{2+} enters the mitochondria, increasing metabolic activity and corresponding ROS formation. 4. ROS signal glutathionylation of VMAT, resulting in decreased VMAT function. 5. Reduced DA packaging results in increased intracellular DA. 6. High intracellular DA overwhelms DAT function, resulting in reverse transport.

4.3 Future Directions

This study has implicated the sigma receptor as a regulator of oxidative stress that disrupts normal DA packaging and release. The above experiments were conducted in slice preparation to allow for more accurate mapping of the mechanism. Such experiments are important, but preliminary. In dealing with disorders of DA depletion or DA cell health, all must

be verified in a freely moving animal. Thus, it is a natural segue to take sigma pharmacology into behavioral paradigms. Can an *in vivo* blockade prevent either drug reinstatement or conditioned place preference studies?

Additionally, it would be instructive to determine how long the effects (notably S-glutathionylation of VMAT2 as well as increased ROS formation) of acute methamphetamine last. Is this post-translational modification reversible or does it require new protein to be made?

Furthermore, this study has been focused on the nucleus accumbens core, with basic verification in the shell. However, measuring or understanding DA release in all parts of the striatum is necessary for a transition from rewarding behaviors to habitual behaviors. By this mechanism, amphetamines indiscriminately affect all DA terminals. We would like to determine a relative timeframe in which this happens and determine if different areas of the striatum develop a sensitivity to methamphetamine after behavioral sensitization. Eventually, determining the mechanization of this plasticity would be our ultimate goal.

Based on our results and those of others, we have also established that neuromelanin forms in response to oxidative stress. We are interested to see if the oxidative stress generated by methamphetamine is enough to trigger neuromelanin formation.

Finally, we have determined that METH interacts with the DAT and VMAT indirectly instead of directly as has been shown with amphetamine. Since much of what is known about METH's mechanism of action has been extrapolated from what is known about amphetamine, it would be instructive to determine if the sigma receptor is involved in amphetamine's mechanism of action.

REFERENCES

1. Graham, D.G., *Oxidative pathways for catecholamines in the genesis of neuromelanin and cytotoxic quinones.* Mol Pharmacol, 1978. **14**(4): p. 633-43.
2. Mosca, L., et al., *Melanins from tetrahydroisoquinolines: spectroscopic characteristics, scavenging activity and redox transfer properties.* Free Radic Biol Med, 1998. **24**(1): p. 161-7.
3. Scott C. Steffensen, N.D.S., David M. Hedges, Eun Young Jang, *Addiction*, in *The SAGE Encyclopedia of Theory in Psychology*, H.L. Miller, Editor. 2016, SAGE Publications, Inc.: Thousand Oaks. p. 5-10.
4. Blackburn, J.R., et al., *Increased dopamine metabolism in the nucleus accumbens and striatum following consumption of a nutritive meal but not a palatable non-nutritive saccharin solution.* Pharmacol Biochem Behav, 1986. **25**(5): p. 1095-100.
5. Wise, R.A. and M.A. Bozarth, *A psychostimulant theory of addiction.* Psychol. Rev., 1987. **94**(1-24).
6. Koob, G.F., *Dopamine, addiction and reward.* Semin. Neurosci., 1992. **4**: p. 139-148.
7. Wise, R.A., *Addictive drugs and brain stimulation reward.* Annu. Rev. Neurosci., 1996. **19**: p. 319-340.
8. McKinzie, D.L., et al., *Cocaine is self-administered into the shell region of the nucleus accumbens in Wistar rats.* 1999. **877**: p. 788-791.
9. Pierce, R.C. and V. Kumaresan, *The mesolimbic dopamine system: the final common pathway for the reinforcing effect of drugs of abuse?* Neurosci Biobehav Rev, 2006. **30**(2): p. 215-38.
10. Yamaguchi, T., W. Sheen, and M. Morales, *Glutamatergic neurons are present in the rat ventral tegmental area.* Eur J Neurosci, 2007. **25**(1): p. 106-18.
11. Margolis, E.B., et al., *The ventral tegmental area revisited: is there an electrophysiological marker for dopaminergic neurons?* J Physiol, 2006. **577**(Pt 3): p. 907-24.
12. Margolis, E.B., et al., *Identification of rat ventral tegmental area GABAergic neurons.* PLoS One, 2012. **7**(7): p. e42365.
13. Ikemoto, S., *Dopamine reward circuitry: Two projection systems from the ventral midbrain to the nucleus accumbens-olfactory tubercle complex.* Brain Res Rev, 2007. **56**(1): p. 27-78.
14. Carlezon, W.A., Jr., D.P. Devine, and R.A. Wise, *Habit-forming actions of nomifensine in nucleus accumbens.* Psychopharmacology (Berl), 1995. **122**(2): p. 194-7.
15. Ikemoto, S., et al., *Role of dopamine D1 and D2 receptors in the nucleus accumbens in mediating reward.* J Neurosci, 1997. **17**(21): p. 8580-7.

16. Rodd-Henricks, Z.A., et al., *Cocaine is self-administered into the shell but not the core of the nucleus accumbens of Wistar rats.* J Pharmacol Exp Ther, 2002. **303**(3): p. 1216-26.
17. Sellings, L.H. and P.B. Clarke, *Segregation of amphetamine reward and locomotor stimulation between nucleus accumbens medial shell and core.* J Neurosci, 2003. **23**(15): p. 6295-303.
18. Sellings, L.H., L.E. McQuade, and P.B. Clarke, *Characterization of dopamine-dependent rewarding and locomotor stimulant effects of intravenously-administered methylphenidate in rats.* Neuroscience, 2006. **141**(3): p. 1457-68.
19. Sellings, L.H., L.E. McQuade, and P.B. Clarke, *Evidence for multiple sites within rat ventral striatum mediating cocaine-conditioned place preference and locomotor activation.* J Pharmacol Exp Ther, 2006. **317**(3): p. 1178-87.
20. Parkinson, J.A., et al., *Disconnection of the anterior cingulate cortex and nucleus accumbens core impairs Pavlovian approach behavior: further evidence for limbic cortical-ventral striatopallidal systems.* Behav Neurosci, 2000. **114**(1): p. 42-63.
21. Ito, R., T.W. Robbins, and B.J. Everitt, *Differential control over cocaine-seeking behavior by nucleus accumbens core and shell.* Nat Neurosci, 2004. **7**(4): p. 389-97.
22. Hernandez, P.J., K. Sadeghian, and A.E. Kelley, *Early consolidation of instrumental learning requires protein synthesis in the nucleus accumbens.* Nat Neurosci, 2002. **5**(12): p. 1327-31.
23. Cardinal, R.N. and T.H. Cheung, *Nucleus accumbens core lesions retard instrumental learning and performance with delayed reinforcement in the rat.* BMC Neurosci, 2005. **6**: p. 9.
24. Parkinson, J.A., et al., *Dissociation in effects of lesions of the nucleus accumbens core and shell on appetitive pavlovian approach behavior and the potentiation of conditioned reinforcement and locomotor activity by D-amphetamine.* J Neurosci, 1999. **19**(6): p. 2401-11.
25. Corbit, L.H., J.L. Muir, and B.W. Balleine, *The role of the nucleus accumbens in instrumental conditioning: Evidence of a functional dissociation between accumbens core and shell.* J Neurosci, 2001. **21**(9): p. 3251-60.
26. Salgado, S. and M.G. Kaplitt, *The Nucleus Accumbens: A Comprehensive Review.* Stereotact Funct Neurosurg, 2015. **93**(2): p. 75-93.
27. David, V., et al., *Rewarding effects elicited by cocaine microinjections into the ventral tegmental area of C57BL/6 mice: involvement of dopamine D1 and serotonin1B receptors.* Psychopharmacology (Berl), 2004. **174**(3): p. 367-75.
28. Rodd, Z.A., et al., *Intracranial self-administration of cocaine within the posterior ventral tegmental area of Wistar rats: evidence for involvement of serotonin-3 receptors and dopamine neurons.* J Pharmacol Exp Ther, 2005. **313**(1): p. 134-45.
29. Gatto, G.J., et al., *Ethanol self-infusion into the ventral tegmental area by alcohol-preferring rats.* Alcohol, 1994. **11**(6): p. 557-64.
30. Rodd-Henricks, Z.A., et al., *Regional heterogeneity for the intracranial self-administration of ethanol within the ventral tegmental area of female Wistar rats.* Psychopharmacology (Berl), 2000. **149**(3): p. 217-24.
31. Gotti, C., et al., *Nicotinic acetylcholine receptors in the mesolimbic pathway: primary role of ventral tegmental area alpha6beta2* receptors in mediating systemic nicotine effects on dopamine release, locomotion, and reinforcement.* J Neurosci, 2010. **30**(15): p. 5311-25.

32. Pons, S., et al., *Crucial role of alpha4 and alpha6 nicotinic acetylcholine receptor subunits from ventral tegmental area in systemic nicotine self-administration.* J Neurosci, 2008. **28**(47): p. 12318-27.
33. Brunzell, D.H., et al., *Alpha-conotoxin MII-sensitive nicotinic acetylcholine receptors in the nucleus accumbens shell regulate progressive ratio responding maintained by nicotine.* Neuropsychopharmacology, 2010. **35**(3): p. 665-73.
34. Zangen, A., et al., *Two brain sites for cannabinoid reward.* J Neurosci, 2006. **26**(18): p. 4901-7.
35. Bozarth, M.A. and R.A. Wise, *Intracranial self-administration of morphine into the ventral tegmental area.* Life Sci., 1981. **28**: p. 551-555.
36. Welzl, H., G. Kuhn, and J.P. Huston, *Self-administration of small amounts of morphine through glass micropipettes into the ventral tegmental area of the rat.* Neuropharmacology, 1989. **28**(10): p. 1017-23.
37. David, V. and P. Cazala, *A comparative study of self-administration of morphine into the amygdala and the ventral tegmental area in mice.* Behav Brain Res, 1994. **65**(2): p. 205-11.
38. Devine, D.P. and R.A. Wise, *Self-administration of morphine, DAMGO, and DPDPE into the ventral tegmental area of rats.* J. Neurosci., 1994. **14**: p. 1978-84.
39. Hyman, S.E. and R.C. Malenka, *Addiction and the brain: the neurobiology of compulsion and its persistence.* Nat Rev Neurosci, 2001. **2**(10): p. 695-703.
40. Hyman, S.E., R.C. Malenka, and E.J. Nestler, *Neural Mechanisms of Addiction: The Role of Reward-Related Learning and Memory.* Annu Rev Neurosci, 2006.
41. Kauer, J.A. and R.C. Malenka, *Synaptic plasticity and addiction.* Nat Rev Neurosci, 2007. **8**(11): p. 844-58.
42. Nugent, F.S. and J.A. Kauer, *LTP of GABAergic synapses in the ventral tegmental area and beyond.* J Physiol, 2008. **586**(6): p. 1487-93.
43. Rothman, R.B., et al., *Amphetamine-type central nervous system stimulants release norepinephrine more potently than they release dopamine and serotonin.* Synapse, 2001. **39**(1): p. 32-41.
44. Shoblock, J.R., et al., *Neurochemical and behavioral differences between d-methamphetamine and d-amphetamine in rats.* Psychopharmacology (Berl), 2003. **165**(4): p. 359-69.
45. Volkow, N.D., et al., *Dopamine in drug abuse and addiction: results from imaging studies and treatment implications.* Mol Psychiatry, 2004. **9**(6): p. 557-69.
46. Volkow, N.D., G.F. Koob, and A.T. McLellan, *Neurobiologic Advances from the Brain Disease Model of Addiction.* N Engl J Med, 2016. **374**(4): p. 363-71.
47. Faure, A., et al., *Lesion to the nigrostriatal dopamine system disrupts stimulus-response habit formation.* J Neurosci, 2005. **25**(11): p. 2771-80.
48. Everitt, B.J. and T.W. Robbins, *From the ventral to the dorsal striatum: devolving views of their roles in drug addiction.* Neurosci Biobehav Rev, 2013. **37**(9 Pt A): p. 1946-54.
49. Koob, G.F. and N.D. Volkow, *Neurocircuitry of addiction.* Neuropsychopharmacology, 2010. **35**(1): p. 217-38.
50. Kimura, M., *Fluorescence histochemical study on serotonin and catecholamine in some plants.* Jpn J Pharmacol, 1968. **18**(2): p. 162-8.
51. Smith, T.A., *Phenethylamine and Related Compounds in Plants.* Phytochemistry, 1977. **16**(1): p. 9-18.

52. University, W. *Enzymatic Browning*. 2014 [cited 2014 7/22/2014]; Available from: http://www.food-info.net/uk/colour/enzymaticbrowning.htm.
53. Solomon, E.I., et al., *Oxygen Binding, Activation, and Reduction to Water by Copper Proteins.* Angew Chem Int Ed Engl, 2001. **40**(24): p. 4570-4590.
54. Lin, C.S. and F.G. Zak, *Studies on melanocytes. VI. Melanocytes in the middle ear.* Arch Otolaryngol, 1982. **108**(8): p. 489-90.
55. Fritz, M.A., et al., *Extracellular and intracellular melanin in inflammatory middle ear disease.* Laryngoscope, 2014. **124**(6): p. E241-4.
56. Curtis, J.L. and L.J. Rubinstein, *Pigmented olfactory neuroblastoma: a new example of melanotic neuroepithelial neoplasm.* Cancer, 1982. **49**(10): p. 2136-43.
57. Chen, H., *Atlas of Genetic Diagnosis and Counseling*. 2006: Humana Press.
58. Tapia, C.V., et al., *Melanocytes and melanin represent a first line of innate immunity against Candida albicans.* Med Mycol, 2014. **52**(5): p. 445-54.
59. Meyskens, F.L., Jr., P.J. Farmer, and H. Anton-Culver, *Etiologic pathogenesis of melanoma: a unifying hypothesis for the missing attributable risk.* Clin Cancer Res, 2004. **10**(8): p. 2581-3.
60. Barden, H. and S. Levine, *Histochemical observations on rodent brain melanin.* Brain Res Bull, 1983. **10**(6): p. 847-51.
61. Fedorow, H., et al., *Neuromelanin in human dopamine neurons: comparison with peripheral melanins and relevance to Parkinson's disease.* Prog Neurobiol, 2005. **75**(2): p. 109-24.
62. Jankovic, J., *Parkinson's disease: clinical features and diagnosis.* J Neurol Neurosurg Psychiatry, 2008. **79**(4): p. 368-76.
63. Dauer, W. and S. Przedborski, *Parkinson's disease: mechanisms and models.* Neuron, 2003. **39**(6): p. 889-909.
64. Mann, D.M. and P.O. Yates, *Possible role of neuromelanin in the pathogenesis of Parkinson's disease.* Mech Ageing Dev, 1983. **21**(2): p. 193-203.
65. Gibb, W.R. and A.J. Lees, *Anatomy, pigmentation, ventral and dorsal subpopulations of the substantia nigra, and differential cell death in Parkinson's disease.* J Neurol Neurosurg Psychiatry, 1991. **54**(5): p. 388-96.
66. Zareba, M., et al., *The Effect of a Synthetic Neuromelanin on Yield of Free Hydroxyl Radicals Generated in Model Systems.* Biochimica Et Biophysica Acta-Molecular Basis of Disease, 1995. **1271**(2-3): p. 343-348.
67. Zecca, L., et al., *A proposed dual role of neuromelanin in the pathogenesis of Parkinson's disease.* Neurology, 2006. **67**(7 Suppl 2): p. S8-11.
68. Li, S.W., et al., *3,4-Dihydroxyphenylacetaldehyde and hydrogen peroxide generate a hydroxyl radical: possible role in Parkinson's disease pathogenesis.* Brain Res Mol Brain Res, 2001. **93**(1): p. 1-7.
69. Burke, W.J., et al., *3,4-Dihydroxyphenylacetaldehyde is the toxic dopamine metabolite in vivo: implications for Parkinson's disease pathogenesis.* Brain Res, 2003. **989**(2): p. 205-13.
70. Koeppen, A.H., *The history of iron in the brain.* J Neurol Sci, 1995. **134 Suppl**: p. 1-9.
71. Visanji, N.P., et al., *Iron deficiency in parkinsonism: region-specific iron dysregulation in Parkinson's disease and multiple system atrophy.* J Parkinsons Dis, 2013. **3**(4): p. 523-37.

72. Oh, E.S., et al., *Hyperspectral fluorescence imaging for cellular iron mapping in the in vitro model of Parkinson's disease.* J Biomed Opt, 2014. **19**(5): p. 051207.
73. Winterbourn, C.C., *Toxicity of iron and hydrogen peroxide: the Fenton reaction.* Toxicol Lett, 1995. **82-83**: p. 969-74.
74. Zecca, L., et al., *Neuromelanin can protect against iron-mediated oxidative damage in system modeling iron overload of brain aging and Parkinson's disease.* J Neurochem, 2008. **106**(4): p. 1866-75.
75. Double, K.L., et al., *Iron-binding characteristics of neuromelanin of the human substantia nigra.* Biochem Pharmacol, 2003. **66**(3): p. 489-94.
76. Zecca, L., et al., *Substantia nigra neuromelanin: structure, synthesis, and molecular behaviour.* Mol Pathol, 2001. **54**(6): p. 414-8.
77. Zecca, L., et al., *The role of iron and copper molecules in the neuronal vulnerability of locus coeruleus and substantia nigra during aging.* Proceedings of the National Academy of Sciences of the United States of America, 2004. **101**(26): p. 9843-9848.
78. Volkow, N.D. *Methamphetamine*. The Science of Drug Abuse & Addiction 2013 [cited 2014 August 13, 2014]; Available from: http://www.drugabuse.gov/publications/research-reports/methamphetamine/letter-director.
79. Abuse, N.I.o.D. *Drugfacts: Methamphetamine*. Drugfacts 2014 [cited 2015 December 9]; Available from: http://www.drugabuse.gov/publications/drugfacts/methamphetamine.
80. Siciliano, C.A., et al., *Biphasic mechanisms of amphetamine action at the dopamine terminal.* J Neurosci, 2014. **34**(16): p. 5575-82.
81. McFadden, L.M., et al., *Prior methamphetamine self-administration attenuates the dopaminergic deficits caused by a subsequent methamphetamine exposure.* Neuropharmacology, 2015. **93**: p. 146-54.
82. Fleckenstein, A.E., T.J. Volz, and G.R. Hanson, *Psychostimulant-induced alterations in vesicular monoamine transporter-2 function: neurotoxic and therapeutic implications.* Neuropharmacology, 2009. **56 Suppl 1**: p. 133-8.
83. Chu, P.W., et al., *Differential regional effects of methamphetamine on dopamine transport.* Eur J Pharmacol, 2008. **590**(1-3): p. 105-10.
84. Rothman, R.B. and M.H. Baumann, *Monoamine transporters and psychostimulant drugs.* Eur J Pharmacol, 2003. **479**(1-3): p. 23-40.
85. Han, D.D. and H.H. Gu, *Comparison of the monoamine transporters from human and mouse in their sensitivities to psychostimulant drugs.* BMC Pharmacol, 2006. **6**: p. 6.
86. Eshleman, A.J., et al., *Release of Dopamine Via the Human Transporter.* Molecular Pharmacology, 1994. **45**(2): p. 312-316.
87. Sitte, H.H., et al., *Carrier-mediated release, transport rates, and charge transfer induced by amphetamine, tyramine, and dopamine in mammalian cells transfected with the human dopamine transporter.* J Neurochem, 1998. **71**(3): p. 1289-97.
88. Jones, S.R., et al., *Profound neuronal plasticity in response to inactivation of the dopamine transporter.* Proc Natl Acad Sci U S A, 1998. **95**(7): p. 4029-34.
89. Jones, S.R., et al., *Mechanisms of amphetamine action revealed in mice lacking the dopamine transporter.* 1998. **18**(6): p. 1979-1986.
90. Sulzer, D., C. St Remy, and S. Rayport, *Reserpine inhibits amphetamine action in ventral midbrain culture.* Mol Pharmacol, 1996. **49**(2): p. 338-42.

91. Peter, D., et al., *The chromaffin granule and synaptic vesicle amine transporters differ in substrate recognition and sensitivity to inhibitors.* J Biol Chem, 1994. **269**(10): p. 7231-7.
92. Brown, J.M., et al., *A single methamphetamine administration rapidly decreases vesicular dopamine uptake.* 2002. **302**(2): p. 497-501.
93. Ritz, M.C., et al., *Cocaine receptors on dopamine transporters are related to self-administration of cocaine.* Science, 1987. **237**(4819): p. 1219-23.
94. Katz, J.L., et al., *A Role for Sigma Receptors in Stimulant Self Administration and Addiction.* Pharmaceuticals (Basel), 2011. **4**(6): p. 880-914.
95. Nguyen, L., et al., *Sigma receptors as potential therapeutic targets for neuroprotection.* Eur J Pharmacol, 2014. **743**: p. 42-7.
96. Su, T.P., et al., *The sigma-1 receptor chaperone as an inter-organelle signaling modulator.* Trends Pharmacol Sci, 2010. **31**(12): p. 557-66.
97. Fukunaga, K., Y. Shinoda, and H. Tagashira, *The role of SIGMAR1 gene mutation and mitochondrial dysfunction in amyotrophic lateral sclerosis.* J Pharmacol Sci, 2015. **127**(1): p. 36-41.
98. Kaushal, N., et al., *AC927, a sigma receptor ligand, blocks methamphetamine-induced release of dopamine and generation of reactive oxygen species in NG108-15 cells.* Mol Pharmacol, 2012. **81**(3): p. 299-308.
99. Hiranita, T., et al., *Stimulants as specific inducers of dopamine-independent sigma agonist self-administration in rats.* J Pharmacol Exp Ther, 2013. **347**(1): p. 20-9.
100. Robinson, D.L., et al., *Disparity between tonic and phasic ethanol-induced dopamine increases in the nucleus accumbens of rats.* Alcohol Clin Exp Res, 2009. **33**(7): p. 1187-96.
101. Justice, J.B., Jr., *Quantitative microdialysis of neurotransmitters.* J Neurosci Methods, 1993. **48**(3): p. 263-76.
102. Yorgason, J.T., et al., *Frequency-Dependent Effects of Ethanol on Dopamine Release in the Nucleus Accumbens.* Alcohol Clin Exp Res, 2013.
103. Robinson, J.D., et al., *Methamphetamine-induced neurotoxicity disrupts pharmacologically evoked dopamine transients in the dorsomedial and dorsolateral striatum.* Neurotox Res, 2014. **26**(2): p. 152-67.
104. Howard, C.D., et al., *Methamphetamine-induced neurotoxicity disrupts naturally occurring phasic dopamine signaling.* Eur J Neurosci, 2013. **38**(1): p. 2078-88.
105. Howard, C.D., et al., *Methamphetamine neurotoxicity decreases phasic, but not tonic, dopaminergic signaling in the rat striatum.* J Neurochem, 2011. **118**(4): p. 668-76.
106. Rebec, G.V., S.J. Barton, and M.D. Ennis, *Dysregulation of ascorbate release in the striatum of behaving mice expressing the Huntington's disease gene.* Journal of Neuroscience, 2002. **22**(2).
107. Peraile, I., et al., *Cocaine potentiates MDMA-induced oxidative stress but not dopaminergic neurotoxicity in mice: implications for the pathogenesis of free radical-induced neurodegenerative disorders.* Psychopharmacology (Berl), 2013. **230**(1): p. 125-35.
108. Macedo, D.S., et al., *Cocaine alters catalase activity in prefrontal cortex and striatum of mice.* Neurosci Lett, 2005. **387**(1): p. 53-6.
109. Numa, R., et al., *Tempol diminishes cocaine-induced oxidative damage and attenuates the development and expression of behavioral sensitization.* Neuroscience, 2008. **155**(3): p. 649-58.

110. Levi, S. and D. Finazzi, *Neurodegeneration with brain iron accumulation: update on pathogenic mechanisms.* Front Pharmacol, 2014. **5**: p. 99.
111. Kondo, T., T. Ito, and Y. Sugita, *Bromocriptine scavenges methamphetamine-induced hydroxyl radicals and attenuates dopamine depletion in mouse striatum.* 1994. **738**: p. 222-229.
112. Giovanni, A., et al., *Estimating hydroxyl radical content in rat brain using systemic and intraventricular salicylate: impact of methamphetamine.* 1995. **64**(4): p. 1819-1825.
113. Fleckenstein, A.E., et al., *Interaction between hyperthermia and oxygen radical formation in the 5-hydroxytryptaminergic response to a single methamphetamine administration.* 1997. **283**(1): p. 281-285.
114. Fleckenstein, A.E., et al., *Oxygen radicals diminish dopamine transporter function in rat striatum.* 1997. **334**(1): p. 111-114.
115. Estler, C.J., *Dependence on age of methamphetamine-produced changes in thermoregulation and metabolism.* Experientia, 1975. **31**(12): p. 1436-7.
116. Kiyatkin, E.A. and H.S. Sharma, *Acute methamphetamine intoxication: brain hyperthermia, blood-brain barrier, brain edema, and morphological cell abnormalities.* Int Rev Neurobiol, 2009. **88**: p. 65-100.
117. Albers, D.S. and P.K. Sonsalla, *Methamphetamine-induced hyperthermia and dopaminergic neurotoxicity in mice: pharmacological profile of protective and nonprotective agents.* 1995. **275**(3): p. 1104-1114.
118. Sandoval, V., G.R. Hanson, and A.E. Fleckenstein, *Methamphetamine decreases mouse striatal dopamine transporter activity: roles of hyperthermia and dopamine.* Eur J Pharmacol, 2000. **409**(3): p. 265-71.
119. Kageyama, G.H. and M.T. Wong-Riley, *Histochemical localization of cytochrome oxidase in the hippocampus: correlation with specific neuronal types and afferent pathways.* Neuroscience, 1982. **7**(10): p. 2337-61.
120. Rowland, K.C., N.K. Irby, and G.A. Spirou, *Specialized synapse-associated structures within the calyx of Held.* J Neurosci, 2000. **20**(24): p. 9135-44.
121. Ricaurte, G.A., C.R. Schuster, and L.S. Seiden, *Long-term effects of repeated methylamphetamine administration on dopamine and serotonin neurons in the rat brain: a regional study.* Brain Res, 1980. **193**(1): p. 153-63.
122. Riddle, E.L., A.E. Fleckenstein, and G.R. Hanson, *Mechanisms of methamphetamine-induced dopaminergic neurotoxicity.* AAPS J, 2006. **8**(2): p. E413-8.
123. Woolverton, W.L., et al., *Long-term effects of chronic methamphetamine administration in rhesus monkeys.* Brain Res, 1989. **486**(1): p. 73-8.
124. Yorgason, J.T., R.A. Espana, and S.R. Jones, *Demon voltammetry and analysis software: analysis of cocaine-induced alterations in dopamine signaling using multiple kinetic measures.* J Neurosci Methods, 2011. **202**(2): p. 158-64.
125. Uys, S.C.-W.J.R.B.L.B.J. *Improvements in the Mass Spectrometric Detection of S-Glutathionylated Peptides Using Multiple Fragmentation Approaches.* in *American Society for Mass Spectrometry*. 2013. Minneapolis, Minnesota.
126. Omiatek, D.M., et al., *The real catecholamine content of secretory vesicles in the CNS revealed by electrochemical cytometry.* Sci Rep, 2013. **3**: p. 1447.
127. Mateo, Y., et al., *Voltammetric assessment of dopamine clearance in the absence of the dopamine transporter: no contribution of other transporters in core or shell of nucleus accumbens.* J Neurosci Methods, 2004. **140**(1-2): p. 183-7.

128. John, C.E. and S.R. Jones, *Voltammetric characterization of the effect of monoamine uptake inhibitors and releasers on dopamine and serotonin uptake in mouse caudate-putamen and substantia nigra slices.* Neuropharmacology, 2007. **52**(8): p. 1596-605.
129. Sulzer, D., *How addictive drugs disrupt presynaptic dopamine neurotransmission.* Neuron, 2011. **69**(4): p. 628-49.
130. Manczak, M., et al., *Time-course of mitochondrial gene expressions in mice brains: implications for mitochondrial dysfunction, oxidative damage, and cytochrome c in aging.* J Neurochem, 2005. **92**(3): p. 494-504.
131. Kim, D., et al., *NADPH oxidase 2-derived reactive oxygen species in spinal cord microglia contribute to peripheral nerve injury-induced neuropathic pain.* Proc Natl Acad Sci U S A, 2010. **107**(33): p. 14851-6.
132. Nguyen, E.C., et al., *Involvement of sigma (sigma) receptors in the acute actions of methamphetamine: receptor binding and behavioral studies.* Neuropharmacology, 2005. **49**(5): p. 638-45.
133. Itzhak, Y., *Repeated methamphetamine-treatment alters brain sigma receptors.* 1993. **230**(2): p. 243-244.
134. Skrzycki, M. and H. Czeczot, *Multiple protective functions of sigma1 receptor.* Curr Protein Pept Sci, 2014. **15**(8): p. 798-811.
135. Imam, S.Z., et al., *Methamphetamine-induced dopaminergic neurotoxicity: role of peroxynitrite and neuroprotective role of antioxidants and peroxynitrite decomposition catalysts.* 2001. **939**: p. 366-380.
136. Solhi, H., et al., *Oxidative stress and lipid peroxidation in prolonged users of methamphetamine.* Drug Metab Lett, 2014. **7**(2): p. 79-82.
137. Walker, J., et al., *Total antioxidant capacity is significantly lower in cocaine-dependent and methamphetamine-dependent patients relative to normal controls: results from a preliminary study.* Hum Psychopharmacol, 2014. **29**(6): p. 537-43.
138. Volz, T.J., G.R. Hanson, and A.E. Fleckenstein, *Measurement of kinetically resolved vesicular dopamine uptake and efflux using rotating disk electrode voltammetry.* J Neurosci Methods, 2006. **155**(1): p. 109-15.
139. Hider, R.C., et al., *Model Compounds for Microbial Iron-Transport Compounds .4. Further Solution Chemistry and Mossbauer Studies on Iron(Ii) and Iron(Iii) Catechol Complexes.* Inorganica Chimica Acta-Bioinorganic Chemistry, 1983. **80**(1-2): p. 51-56.
140. Mosharov, E.V., et al., *Interplay between cytosolic dopamine, calcium, and alpha-synuclein causes selective death of substantia nigra neurons.* Neuron, 2009. **62**(2): p. 218-29.
141. Lebedev, A.V., et al., *[Paramagnetic calcium melanins].* Biofizika, 2013. **58**(1): p. 47-53.
142. McCord, J.M. and E.D. Day, Jr., *Superoxide-dependent production of hydroxyl radical catalyzed by iron-EDTA complex.* FEBS Lett, 1978. **86**(1): p. 139-42.
143. Schulz, J.B., et al., *Glutathione, oxidative stress and neurodegeneration.* Eur J Biochem, 2000. **267**(16): p. 4904-11.
144. Nakamura, K., W. Wang, and U.J. Kang, *The role of glutathione in dopaminergic neuronal survival.* J Neurochem, 1997. **69**(5): p. 1850-8.
145. Sian, J., et al., *Alterations in glutathione levels in Parkinson's disease and other neurodegenerative disorders affecting basal ganglia.* Ann Neurol, 1994. **36**(3): p. 348-55.

146. Gerlach, M., et al., *Altered brain metabolism of iron as a cause of neurodegenerative diseases?* J Neurochem, 1994. **63**(3): p. 793-807.
147. Galazka-Friedman, J., et al., *Iron in parkinsonian and control substantia nigra--a Mossbauer spectroscopy study.* Mov Disord, 1996. **11**(1): p. 8-16.
148. Gerlach, M., et al., *Mossbauer spectroscopic studies of purified human neuromelanin isolated from the substantia nigra.* J Neurochem, 1995. **65**(2): p. 923-6.
149. Enochs, W.S., M.J. Nilges, and H.M. Swartz, *Purified human neuromelanin, synthetic dopamine melanin as a potential model pigment, and the normal human substantia nigra: characterization by electron paramagnetic resonance spectroscopy.* J Neurochem, 1993. **61**(1): p. 68-79.
150. Perry, T.L., D.V. Godin, and S. Hansen, *Parkinson's disease: a disorder due to nigral glutathione deficiency?* Neurosci Lett, 1982. **33**(3): p. 305-10.
151. Fariello, R.G., et al., *Regional distribution of ubiquinones and tocopherols in the mouse brain: lowest content of ubiquinols in the substantia nigra.* Neuropharmacology, 1988. **27**(10): p. 1077-80.
152. Owesson-White, C.A., et al., *Sources contributing to the average extracellular concentration of dopamine in the nucleus accumbens.* J Neurochem, 2012. **121**(2): p. 252-62.
153. Sombers, L.A., et al., *Synaptic overflow of dopamine in the nucleus accumbens arises from neuronal activity in the ventral tegmental area.* J Neurosci, 2009. **29**(6): p. 1735-42.
154. Zweifel, L.S., et al., *Disruption of NMDAR-dependent burst firing by dopamine neurons provides selective assessment of phasic dopamine-dependent behavior.* Proc Natl Acad Sci U S A, 2009. **106**(18): p. 7281-8.
155. Wyvell, C.L. and K.C. Berridge, *Intra-accumbens amphetamine increases the conditioned incentive salience of sucrose reward: enhancement of reward "wanting" without enhanced "liking" or response reinforcement.* J Neurosci, 2000. **20**(21): p. 8122-30.
156. Knutson, B., et al., *Amphetamine modulates human incentive processing.* Neuron, 2004. **43**(2): p. 261-9.
157. Ingram, S.L., B.M. Prasad, and S.G. Amara, *Dopamine transporter-mediated conductances increase excitability of midbrain dopamine neurons.* Nat Neurosci, 2002. **5**(10): p. 971-8.
158. Schmitz, Y., et al., *Amphetamine distorts stimulation-dependent dopamine overflow: effects on D2 autoreceptors, transporters, and synaptic vesicle stores.* J Neurosci, 2001. **21**(16): p. 5916-24.
159. Maurice, T. and T.P. Su, *The pharmacology of sigma-1 receptors.* Pharmacol Ther, 2009. **124**(2): p. 195-206.
160. Matsumoto, R.R., et al., *Sigma (sigma) receptors as potential therapeutic targets to mitigate psychostimulant effects.* Adv Pharmacol, 2014. **69**: p. 323-86.
161. Zeng, C., et al., *Subcellular localization of sigma-2 receptors in breast cancer cells using two-photon and confocal microscopy.* Cancer Res, 2007. **67**(14): p. 6708-16.
162. Alonso, G., et al., *Immunocytochemical localization of the sigma(1) receptor in the adult rat central nervous system.* Neuroscience, 2000. **97**(1): p. 155-70.
163. Hayashi, T. and T.P. Su, *Sigma-1 receptor chaperones at the ER-mitochondrion interface regulate Ca(2+) signaling and cell survival.* Cell, 2007. **131**(3): p. 596-610.

164. Pal, A., et al., *The sigma-1 receptor protects against cellular oxidative stress and activates antioxidant response elements.* Eur J Pharmacol, 2012. **682**(1-3): p. 12-20.
165. Wang, L., et al., *Sigma 1 receptor stimulation protects against oxidative damage through suppression of the ER stress responses in the human lens.* Mech Ageing Dev, 2012. **133**(11-12): p. 665-74.
166. Bucolo, C., et al., *Sigma receptor ligands protect human retinal cells against oxidative stress.* Neuroreport, 2006. **17**(3): p. 287-91.
167. Matsumoto, R.R., et al., *Attenuation of methamphetamine-induced effects through the antagonism of sigma (sigma) receptors: Evidence from in vivo and in vitro studies.* Eur Neuropsychopharmacol, 2008. **18**(12): p. 871-81.
168. Potula, R., et al., *Methamphetamine causes mitrochondrial oxidative damage in human T lymphocytes leading to functional impairment.* J Immunol, 2010. **185**(5): p. 2867-76.
169. Contreras, L., et al., *Mitochondria: the calcium connection.* Biochim Biophys Acta, 2010. **1797**(6-7): p. 607-18.
170. Annunziata, I. and A. d'Azzo, *Interorganellar membrane microdomains: dynamic platforms in the control of calcium signaling and apoptosis.* Cells, 2013. **2**(3): p. 574-90.
171. Barr, J.L., et al., *Mechanisms of activation of nucleus accumbens neurons by cocaine via sigma-1 receptor-inositol 1,4,5-trisphosphate-transient receptor potential canonical channel pathways.* Cell Calcium, 2015. **58**(2): p. 196-207.
172. Novakova, M., et al., *Highly selective sigma receptor ligands elevate inositol 1,4,5-trisphosphate production in rat cardiac myocytes.* Eur J Pharmacol, 1998. **353**(2-3): p. 315-27.
173. Zhang, C.L., et al., *Methylphenidate enhances NMDA-receptor response in medial prefrontal cortex via sigma-1 receptor: a novel mechanism for methylphenidate action.* PLoS One, 2012. **7**(12): p. e51910.
174. Barayuga, S.M., et al., *Methamphetamine decreases levels of glutathione peroxidases 1 and 4 in SH-SY5Y neuronal cells: protective effects of selenium.* Neurotoxicology, 2013. **37**: p. 240-6.
175. Horner, K.A., Y.E. Gilbert, and S.D. Cline, *Widespread increases in malondialdehyde immunoreactivity in dopamine-rich and dopamine-poor regions of rat brain following multiple, high doses of methamphetamine.* Front Syst Neurosci, 2011. **5**: p. 27.
176. Huang, M.C., et al., *Oxidative stress status in recently abstinent methamphetamine abusers.* Psychiatry Clin Neurosci, 2013. **67**(2): p. 92-100.
177. Barbosa, D.J., et al., *Mitochondria: key players in the neurotoxic effects of amphetamines.* Arch Toxicol, 2015. **89**(10): p. 1695-725.
178. Chatterjee, P.K., et al., *Tempol, a membrane-permeable radical scavenger, reduces oxidant stress-mediated renal dysfunction and injury in the rat.* Kidney Int, 2000. **58**(2): p. 658-73.
179. Shiba, T., et al., *In vivo imaging of mitochondrial function in methamphetamine-treated rats.* Neuroimage, 2011. **57**(3): p. 866-72.
180. Yu, S., et al., *Recent advances in methamphetamine neurotoxicity mechanisms and its molecular pathophysiology.* Behav Neurol, 2015. **2015**: p. 103969.
181. Uys, J.D., P.J. Mulholland, and D.M. Townsend, *Glutathione and redox signaling in substance abuse.* Biomed Pharmacother, 2014. **68**(6): p. 799-807.
182. Rossi, R., et al., *Protein S-glutathionylation and platelet anti-aggregating activity of disulfiram.* Biochem Pharmacol, 2006. **72**(5): p. 608-15.

183. Floor, E., P.S. Leventhal, and S.F. Schaeffer, *Partial purification and characterization of the vacuolar H(+)-ATPase of mammalian synaptic vesicles.* J Neurochem, 1990. **55**(5): p. 1663-70.
184. Freyberg, Z., et al., *Mechanisms of amphetamine action illuminated through optical monitoring of dopamine synaptic vesicles in Drosophila brain.* Nat Commun, 2016. **7**: p. 10652.
185. LaVoie, M.J. and T.G. Hastings, *Dopamine quinone formation and protein modification associated with the striatal neurotoxicity of methamphetamine: evidence against a role for extracellular dopamine.* J Neurosci, 1999. **19**(4): p. 1484-91.
186. Kita, T., et al., *Hydroxyl radical formation following methamphetamine administration to rats.* Pharmacol Toxicol, 1999. **85**(3): p. 133-7.
187. Casida, J.E., et al., *Benomyl, aldehyde dehydrogenase, DOPAL, and the catecholaldehyde hypothesis for the pathogenesis of Parkinson's disease.* Chem Res Toxicol, 2014. **27**(8): p. 1359-61.
188. Lohr, K.M., et al., *Increased Vesicular Monoamine Transporter 2 (VMAT2; Slc18a2) Protects against Methamphetamine Toxicity.* ACS Chem Neurosci, 2015. **6**(5): p. 790-9.
189. Johanson, C.E., et al., *Cognitive function and nigrostriatal markers in abstinent methamphetamine abusers.* Psychopharmacology (Berl), 2006. **185**(3): p. 327-38.
190. Bellinger, F.P., et al., *Regulation and function of selenoproteins in human disease.* Biochem J, 2009. **422**(1): p. 11-22.